Commun. Comput. Phys.
doi: 10.4208/cicp.OA-2022-0204

Vol. **33**, No. 3, pp. 733-763
March 2023

The Bulk-Surface Virtual Element Method for Reaction-Diffusion PDEs: Analysis and Applications

Massimo Frittelli[1,*], Anotida Madzvamuse[2,3,4] and Ivonne Sgura[1]

[1] *Department of Mathematics and Physics "E. De Giorgi", University of Salento, Via per Arnesano, 73100 Lecce, Italy.*
[2] *Department of Mathematics, University of British Columbia, 1984 Mathematics Road, Vancouver, BC V6T 1Z2, Canada.*
[3] *Department of Mathematics, School of Mathematical and Physical Sciences, University of Sussex, Brighton, BN1 9QH, UK.*
[4] *Department of Mathematics and Applied Mathematics, University of Pretoria, Private Bag x 20, Hatfield, 0028, South Africa.*

Received 27 July 2022; Accepted (in revised version) 4 December 2022

Abstract. Bulk-surface partial differential equations (BS-PDEs) are prevalent in many applications such as cellular, developmental and plant biology as well as in engineering and material sciences. Novel numerical methods for BS-PDEs in three space dimensions (3D) are sparse. In this work, we present a bulk-surface virtual element method (BS-VEM) for bulk-surface reaction-diffusion systems, a form of semilinear parabolic BS-PDEs in 3D. Unlike previous studies in two space dimensions (2D), the 3D bulk is approximated with general polyhedra, whose outer faces constitute a flat polygonal approximation of the surface. For this reason, the method is restricted to the lowest order case where the geometric error is not dominant. The BS-VEM guarantees all the advantages of polyhedral methods such as easy mesh generation and fast matrix assembly on general geometries. Such advantages are much more relevant than in 2D. Despite allowing for general polyhedra, general nonlinear reaction kinetics and general surface curvature, the method only relies on nodal values without needing additional evaluations usually associated with the quadrature of general reaction kinetics. This latter is particularly costly in 3D. The BS-VEM as implemented in this study retains optimal convergence of second order in space.

AMS subject classifications: 35K57, 65M12, 65M15, 65M20, 65M50, 65M60

Key words: Bulk-surface PDEs, bulk-surface reaction-diffusion systems, polyhedral meshes, bulk-surface virtual element method, convergence.

*Corresponding author. *Email addresses:* massimo.frittelli@unisalento.it (M. Frittelli), am823@math.ubc.ca (A. Madzvamuse), ivonne.sgura@unisalento.it (I. Sgura)

1 Introduction

Bulk-surface partial differential equations (BS-PDEs) arise from a wide variety of real-life problems. They describe many natural problems including, but are not limited to, the formation of spatial patterning in developmental biology [46], cell polarisation in molecular and cellular biology [18, 26, 33, 45, 50], fluid dynamics [17, 20, 44], the formation of an appressorium by the infection of the fungus *Magnaporthe grisea* causing rice blast [52], spine growth in sea urchins [43], root formation and food uptake in plant biology [5], and so on. Given the complex nature of BS-PDEs, their numerical treatment is generally not trivial, in particular in three space dimensions (3D). Hence, developing novel numerical methods and constructing stable and accurate algorithms to approximate their numerical solutions becomes crucially important, given their rapid applications to areas such as biomedical engineering, fluid dynamics, materials science, biology, cancer biology, image processing, astrophysics and battery modeling, to mention just a few examples.

Given $d \in \mathbb{N}$ denoting the number of space dimensions, a bulk-surface reaction-diffusion system (BS-RDS) comprises of $m \in \mathbb{N}$ reaction-diffusion equations (RDEs) posed in the *bulk* domain $\Omega \subset \mathbb{R}^d$ $(d \geq 2)$ coupled, through either linear or non-linear mixed Robin-type boundary conditions, with $n \in \mathbb{N}$ surface RDEs posed on the manifold $\Gamma := \partial\Omega$. The generalised BS-RDS takes the following form:

$$\begin{cases} \dot{u}_i - d_{u,i}\Delta u_i = q_i(u_1,\cdots,u_m), & \boldsymbol{x} \in \Omega; \\ \dot{v}_j - d_{v,j}\Delta_\Gamma v_j + \sum_{k=1}^{m} \eta_{jk} \nabla u_k \cdot \boldsymbol{\nu} = r_j(u_1,\cdots,u_m,v_1,\cdots,v_n), & \boldsymbol{x} \in \Gamma; \\ \nabla u_i \cdot \boldsymbol{\nu} = s_i(u_1,\cdots,u_m,v_1,\cdots,v_n), & \boldsymbol{x} \in \Gamma, \end{cases} \tag{1.1}$$

for $i = 1,\cdots,m$, $j = 1,\cdots,n$ and $t \in [0,T]$, where $T > 0$ is the final time. In the above, $\dot{u}_i$ and $\dot{v}_j$ denote partial time derivatives. The functions q_i, r_j, s_i are nonlinear reaction kinetics, $d_{u,i}, d_{v,j} > 0$ are the diffusion coefficients and $\eta_{jk} > 0$ are coupling coefficients fulfilling $\sum_{j=1}^{n} \eta_{jk} = d_{u,k}$ for all $k = 1,\cdots,m$, which can be interpreted as a balance law across bulk and surface, see [46]. In (1.1), Δ and Δ_Γ denote the Laplace and Laplace-Beltrami operators respectively, while $\boldsymbol{\nu} : \Gamma \to \mathbb{R}^d$ is the outward unit normal vector field on Γ (see [35] for full definitions). The model comprises several time-dependent BS-PDE models currently existing in the literature, see for example [33, 46, 51]. The BS-VEM builds substantially on the virtual element method (VEM), which in turn, is an extension of the well-known finite element method (FEM) for the numerical approximation of PDEs on flat [8] and 3D domains [49] as well as on surfaces [38].

Several element-based numerical methods have been developed for the spatial discretisation of BS-PDEs; current-state-of-the-art methods existing in the literature include classical finite elements [31, 42, 46, 47], cut finite elements [20], discontinuous Galerkin methods [24], kernel collocation methods [23] and trace finite elements [41]. We seek to contribute to this area by developing the *bulk-surface virtual element method* (BS-VEM)

for the spatial discretisation of coupled systems of BS-PDEs in 3D ($d=3$). The methodology we are proposing combines the classical VEM for bulk equations [10] posed in bulk domains with the surface virtual element method (SVEM) [38] for the surface equations posed on closed manifolds. This method is a substantial extension of our previous work on the two-dimensional ($d=2$) BS-VEM introduced in [34]. Unlike our previous work presented in [34] where the surface PDEs were solved using the surface finite element method, in this work, we employ virtual elements for both bulk and surface PDEs. The BS-VEM we propose relies on an arbitrary polyhedral discretisation of the bulk domain, while the surface polygonation is taken as the boundary of the bulk polyhedration thereby giving rise to a polygonal approximation of the surface. Crucial in this regard is the property that *the 2D VEM space on each 2D face is the trace of the 3D VEM space on a polyhedral element*, i.e. higher dimensional VEM spaces are constructed recursively from lower dimensional spaces. To demonstrate the generality and applicability of our numerical approach, we apply the BS-VEM to the BS-RDS (1.1). The BS-RDSs cover a wide range of models prevalently studied in the literature, see for instance [26,33,46].

The main novelty of our study is devoted to numerical error analysis. It turns out that the simultaneous presence of non-tetrahedral elements in the bulk and surface introduce approximation errors which provide new challenges for the numerical analysis of the BS-PDEs. We note that the surface approximation error cannot be neglected in the context of BS-PDEs, because the surface itself is the domain for the surface PDEs. We prove that, in space, the BS-VEM possesses optimal second-order convergence provided the exact solution is $H^{2+\frac{3}{4}}$ in the bulk domain and H^2 on the surface. It must be observed that this requirement is more than the usual H^2 regularity required by the BS-FEM [42] for both in the bulk and on the surface. Furthermore, this requirement is also more than the $H^{2+1/4}$ regularity required by the BS-VEM in the 2D case [34]. The rationale for this is due to Sobolev embeddings being more restrictive in 3D. The novelty here is that our analysis requires this higher regularity assumption only *in the simultaneous presence of a curved boundary* Γ *and non-tetrahedral elements that touch the surface*. Otherwise, our results encompass well-known cases in the literature, see for instance [42] in the case of tetrahedral BSFEM, and [1] for the case of polyhedral VEM in the absence of curvature in the boundary Γ. It must be pointed out that such extra regularity comes for free in most models and applications, where the domains are smooth and the solutions are infinitely differentiable. We also point out that, even if the surface is two dimensional, we require no extra regularity for the surface species, while in the 2D case we had required $H^{2+1/4}$ regularity in the two-dimensional bulk. This point out *the joint role of dimensionality and bulk-surface dichotomy in the error analysis.*

A by-product of our numerical error analysis is that the bulk-VEM of lowest polynomial order $k=1$ possesses optimal convergence *in the presence of curved boundaries*. Even in the special case of simplicial elements (FEM), the error analysis of boundary data is not trivial and is provided in [7]. For general polyhedral elements (VEM), a first work in this direction is [16], where suitable algebraic corrections in the method guarantee optimal convergence even in the presence of curved boundaries. As an alternative approach, the

work in [13] uses curved elements in the 2D case, while 3D VEM elements with curved faces were introduced in [28] for PDEs of mixed form. In this work, we obtain similar results in the low order case $k=1$ by harnessing, in a novel way, the geometric error estimates of bulk-surface polyhedral domains [31]. The BS-VEM proposed here, which does not need algebraic corrections nor curved elements, is fully practical since it relies on vertex-wise degrees of freedom without renouncing optimal convergence.

As in the 2D case [34], our analysis relies on the Stein extension operator as an alternative to the lifting operator commonly adopted in the analysis of SPDEs [30] and BS-PDEs [31]. This choice is dictated by the crucial property that the Stein extension of a function preserves its $W^{m,p}$ class, while lifting does not. The usage of the Stein extension leads to the $H^{2+\frac{3}{4}}$ regularity required for the exact solution in the bulk.

The proposed BS-VEM has all the benefits of polyhedral meshes, summarised as follows. (I) The usage of polyhedra allows for the generation of cut cubic meshes, which for suitable cases is faster than the generation of unstructured tetrahedral meshes, see [34,35]. (II) On such cut cubic meshes, VEM matrix assembly is most likely to be quicker than on unstructured tetrahedral meshes because most elements are equal cubes where the VEM local matrices are known in closed form [34,35]. Of course one could as well apply FEM on cut cubic meshes by considering a sub-tetrahedrisation, but this procedure is discouraged, especially for large-scale or CAD applications where mesh generation takes the vast majority of the computational time of the whole solution process [25]. Similar results are obtained in the literature through other methods, such as trace [41] or cut FEMs [20]. (III) A curved portion of the boundary can be approximated with a single element with many faces. (IV) Thanks to the special treatment of the nonlinear reaction kinetics which we have adapted from [1], the method relies only on nodal values, thus avoiding quadratures on general polyhedra, which can be particularly costly in 3D. This means that the method combines the generality of polyhedral methods with the immediate treatment of nonlinearities of pointwise methods such as lumped finite elements [36,37]. The BS-VEM lends itself to other advantages due to its polyhedral nature, such as (V) efficient mesh-adaptive algorithms or (VI) mesh pasting, see for instance [21]. Some of these aspects form part of our current and future studies.

Hence, the structure of our paper is as follows. In Section 2, we introduce the BS-PDE model to be addressed in the present work: a semi-linear parabolic BS-RDS. We then introduce in the same section the strong and weak formulations of the BS-RDS. In Section 3, we (i) introduce the approximation of the bulk and surface domains based on polyhedral bulk-surface meshes which are the key ingredients for the BS-VEM, (ii) recap the geometric error estimates of polyhedral bulk-surface meshes, (iii) define suitable function spaces and discrete bilinear forms thereby showing their approximation properties and (iv) present the spatial discretisation of the considered BS-PDE problem. In Section 4, we carry out the stability and convergence error analysis. Specifically, our main result is the optimal second-order spatial convergence of the BS-VEM in L^2 norms, both in the bulk and on the surface (Theorem 4.3). In Section 5 we present the IMEX-Euler time-discretisation of the semi-linear parabolic PDE problem. Section 6 demonstrates compu-

tationally the optimal orders of convergence (i.e. second order in space and first order in time) of the BS-VEM-IMEX Euler by presenting two examples: (i) a linear parabolic BS-PDE and (ii) a BS-RDS with activator-depleted reaction kinetics. Both of these BS-PDEs are solved on the unit sphere. We draw conclusions of our work and present future challenges in Section 7. In Appendix A we provide some basic definitions and results required to carry out numerical error analysis.

2 Coupled bulk-surface reaction-diffusion systems

Let $\Omega \subset \mathbb{R}^3$ be an open domain such that its boundary $\Gamma = \partial\Omega$ is a smooth manifold. Let $u(\boldsymbol{x},t)$ and $v(\boldsymbol{x},t)$ be the bulk and surface variables obeying the following *bulk-surface reaction-diffusion system* (BS-RDS):

$$\begin{cases} \dot{u} - d_u \Delta u = q(u), & \boldsymbol{x} \in \Omega, \ t \in [0,T]; \\ \dot{v} - d_v \Delta_\Gamma v + d_u \nabla u \cdot \boldsymbol{\nu} = r(u,v), & \boldsymbol{x} \in \Gamma, \ t \in [0,T]; \\ d_u \nabla u \cdot \boldsymbol{\nu} = s(u,v), & \boldsymbol{x} \in \Gamma, \ t \in [0,T]; \\ u(\boldsymbol{x},0) = u_0(\boldsymbol{x}), & \boldsymbol{x} \in \Omega; \\ v(\boldsymbol{x},0) = v_0(\boldsymbol{x}), & \boldsymbol{x} \in \Gamma, \end{cases} \tag{2.1}$$

where the regularity of Γ, u_0, v_0, q, r, and s is stated below. System (2.1) is the special case of system (1.1) when $m=n=1$. Throughout this work, we will analyse the system (2.1) for ease of presentation. Without loss of generality, the proposed analysis applies to the general case (1.1). To derive a weak formulation of problem (2.1), we multiply the first two equations of (2.1) by two test functions $\varphi \in L^2([0,T];H^1(\Omega))$ and $\psi \in L^2([0,T];H^1(\Gamma))$, respectively. Then we apply Green's formula in the bulk Ω, Green's formula on the curved manifold Γ (see [30]), we substitute the third equation of (2.1) into the second and we exploit the fact that Γ has an empty one-dimensional boundary. We obtain the following formulation: find $u \in L^2([0,T];H^1(\Omega))$, $v \in L^2([0,T];H^1(\Gamma))$ with $\dot{u} \in L^2([0,T];H^{-1}(\Omega))$, $\dot{v} \in L^2([0,T];H^{-1}(\Gamma))$ such that

$$\begin{cases} \displaystyle\int_\Omega \dot{u}\varphi + d_u \int_\Omega \nabla u \cdot \nabla \varphi = \int_\Omega q(u)\varphi + \int_\Gamma s(u,v)\varphi; \\ \displaystyle\int_\Gamma \dot{v}\psi + d_v \int_\Gamma \nabla_\Gamma v \cdot \nabla_\Gamma \psi + \int_\Gamma s(u,v)\psi = \int_\Gamma r(u,v)\psi, \end{cases} \tag{2.2}$$

for all $\varphi \in L^2([0,T];H^1(\Omega))$, $\psi \in L^2([0,T];H^1(\Gamma))$. For the remainder of this work we will adopt the following set of assumptions to ensure that the numerical method is well-posed and stable.

Assumption 1 (Regularity of domain, kinetics, and initial data for problem (2.2))**.** We assume that:

- Γ is a $\mathcal{C}^3$ surface, the functions $q(\cdot)$,$r(\cdot,\cdot)$,$s(\cdot,\cdot)$ are globally Lipschitz.

- The initial datum (u_0,v_0) fulfils $u_0\in H^2(\Omega)$, $\mathrm{Tr}(u_0)\in H^2(\Gamma)$ and $v_0\in H^2(\Gamma)$.

The proposed convergence result (Theorem 4.3) holds true if the exact solution is sufficiently regular. Since, to the best of our knowledge, regularity results for nonlinear BS-PDEs are mostly an uncharted territory, for our purposes we will conjecture that the solution is sufficiently regular, thereby providing some arguments to support our conjecture. A full proof is outside the scope of this work.

Conjecture 1 (Existence, uniqueness, and regularity for problem (2.1))**.** In addition to Assumption 1, assume that the bulk initial datum u_0 fulfils $u_0\in H^{2+\frac{3}{4}}(\Omega)$, then there exists a unique solution (u,v) to problem (2.1) that fulfils

$$u,\dot{u}\in L^2([0,T];H^{2+\frac{3}{4}}(\Omega)) \quad \text{and} \quad \mathrm{Tr}(u),\mathrm{Tr}(\dot{u}),v,\dot{v}\in L^2([0,T];H^2(\Gamma)). \tag{2.3}$$

Arguments. The following arguments support our conjecture. (I) For a stationary elliptic counterpart of the BS-RDS (2.1), an $H^2(\Omega)\times H^2(\Gamma)$ regularity result is known [31, Theorem 3.2]. (II) For bulk-only PDEs on flat domains, high regularity in Bochner spaces follows from the well-known parabolic regularity theory [3]. (III) Standard energy arguments apply straight away to problem (2.1) yielding bounds of the type

$$\begin{aligned} &u\in L^\infty([0,T];H^1(\Omega)), \quad \dot{u}\in L^2([0,T];L^2(\Omega));\\ &v\in L^\infty([0,T];H^1(\Gamma)), \quad \dot{v}\in L^2([0,T];L^2(\Gamma)). \end{aligned}$$

In many applications, assuming globally Lipschitz kinetics is too restrictive and models with non-globally Lipschitz kinetics require ad-hoc analysis, see for instance [33]. However, there are notable examples of BS-RDS models with globally Lipschitz kinetics, such as the wave pinning model studied in [26]. In this work, we shall assume that the weak BS-RDS (2.2) has a unique and sufficiently regular solution (u,v).

3 The bulk-surface virtual element method

In this section we introduce the bulk-surface virtual element method (BS-VEM) for BS-RDSs in 3D of the form (2.1), thereby extending the 2D counterpart introduced in [34] and the 3D elliptic counterpart introduced in [35]. To this end, we start by recalling from [35] the theory of bulk-surface meshes.

3.1 Polyhedral bulk-surface meshes

The starting point is the approximation of the geometry. The reader is referred to [35] for complete details. Let $h>0$ be a positive number called *meshsize*. The bulk domain Ω is approximated with a polyhedral domain Ω_h composed of a collection $\mathcal{E}_h$ of non-degenerate and non-overlapping polyhedra whose diameters do not exceed h. It therefore holds that $\Omega_h=\cup_{E\in\mathcal{E}_h}E$. The polyhedral bulk domain Ω_h induces a polygonal approximation Γ_h

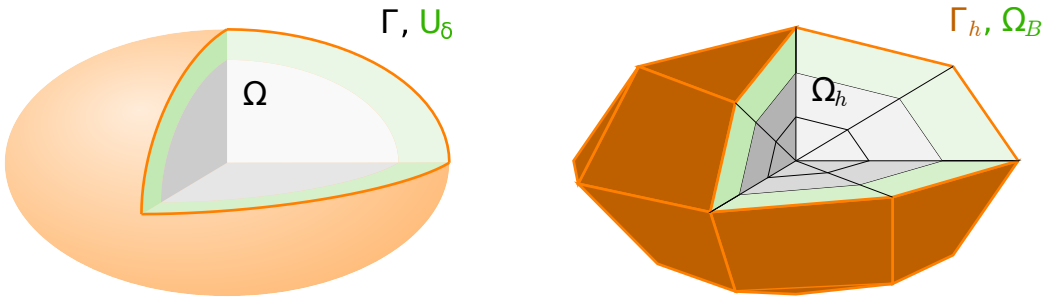

(a) *Bulk* domain Ω enclosed by the *surface* Γ, and *narrow band* U_δ *of width* δ.

(b) *Discrete bulk* domain Ω_h enclosed by the *discrete surface* Γ_h, and *discrete narrow band* Ω_B.

Figure 1: An illustration of (a) the continuous domain, (b) the discrete domain and their related notations.

of Γ, defined by $\Gamma_h = \partial\Omega_h$. We can write $\Gamma_h = \cup_{F\in\mathcal{F}_h} F$, where $\mathcal{F}_h$ is a collection of faces. We assume that the meshes Ω_h and Γ_h fulfil suitable regularity assumptions as detailed in [35]. Let Ω_B be the *discrete narrow band*, made up of the polyhedral elements of $E\in\mathcal{E}_h$ that touch the boundary Γ_h. See Fig. 1 for an illustration.

Let $\boldsymbol{x}_i$, $i=1,\cdots,N\in\mathbb{N}$ be the nodes of Ω_h and assume that the nodes of Γ_h are $\boldsymbol{x}_k$, $k=1,\cdots,M<N$, i.e. the first M nodes of Ω_h. The *reduction matrix* $R\in\mathbb{R}^{N\times M}$ is the upper trapezoidal matrix whose entries R_{ik} are defined as

$$R_{ik}=\begin{cases}\delta_{ik} & \text{for } i=1,\cdots,M;\\ 0 & \text{for } i=M+1,\cdots,N,\end{cases} \tag{3.1}$$

for all $k=1,\cdots,M$, where δ_{ik} is the Kronecker symbol. The usefulness of R stems from the following properties: (i) for any $\boldsymbol{v}\in\mathbb{R}^N$, $R^T\boldsymbol{v}\in\mathbb{R}^M$ is the vector with the first M entries of $\boldsymbol{v}$, and (ii) for any $\boldsymbol{w}\in\mathbb{R}^M$, $R\boldsymbol{w}\in\mathbb{R}^N$ is the vector whose first M entries are those of $\boldsymbol{w}$ and the other $N-M$ entries are 0. We will use the matrix R to formulate the BS-VEM in matrix form. We conclude this section by recalling that suitable bulk-surface polyhedral meshes constructed by cutting a uniform cubic mesh can accelerate mesh generation in suitable cases, see [34,35]. Another advantage is the possibility of accurately representing a heavily curved portion of the boundary by a single element with many edges and faces.

3.2 Variational crime

We report from our paper [35] the geometric error analysis of polyhedral bulk-surface meshes.

Lemma 3.1 (Parametrisation of geometry)**.** *The following statements hold true:*

1. *There exists a homeomorphism $G:\Omega_h\to\Omega$ such that $G\in W^{1,\infty}(\Omega_h)$ and*

$$\|J_G-I\|_{0,\infty,\Omega_B}\leq Ch; \tag{3.2}$$
$$\|\det(J_G)-1\|_{0,\infty,\Omega_B}\leq Ch; \tag{3.3}$$
$$\|G-I\|_{0,\infty,\Omega_B}\leq Ch^2; \tag{3.4}$$
$$G|_{\Gamma_h}=\boldsymbol{a}|_{\Gamma_h}; \tag{3.5}$$
$$G|_{\Omega_h\setminus\Omega_B}=I, \tag{3.6}$$

   where U is a sufficiently narrow open neighborhood of Γ and $\boldsymbol{a}:U\to\Gamma$ is the normal projection onto Γ (see [35]*), J_G is the Jacobian of G, I is the identity matrix, and $C>0$ is a constant that depends on Γ and on the shape regularity of the mesh, see* [35] *for further details.*

2. *Even if restricted to a single element $E\in\mathcal{E}_h$, G might not be a diffeomorphism (i.e. its first derivatives might be discontinuous) unless E is a tetrahedron.*

Definition 3.1 (Bulk- and surface-lifting operators)**.** Given $V:\Omega_h\to\mathbb{R}$ and $W:\Gamma_h\to\mathbb{R}$, their *lifts* are defined by $V^\ell:=V\circ G^{-1}$ and $W^\ell:=W\circ G^{-1}$, respectively. Conversely, given $v:\Omega\to\mathbb{R}$ and $w:\Gamma\to\mathbb{R}$, their *inverse lifts* are defined by $v^{-\ell}:=v\circ G$ and $w^{-\ell}:=w\circ G$, respectively, with $G:\Omega_h\to\Omega$ being the mapping defined in Lemma 3.1.

On one hand, the relations (3.2)-(3.6) of Lemma 3.1 ensure that polyhedral meshes possess the correct approximation properties in terms of convergence rate, analogously to the special case of simplicial meshes (see [31]). On the other hand, the second statement of Lemma 3.1 implies that the $H^s(\Omega)$, $s>1$, regularity class of functions is not preserved under the action of the lifting operators in Definition 3.1, thus motivating the line of analysis adopted throughout this work.

Lemma 3.2 (Equivalence of norms under lifting)**.** *There exist two constants $C>c>0$ depending on Γ and on the shape regularity of the mesh (see* [35]*) such that*

$$c\|V^\ell\|_{0,\Omega}\leq\|V\|_{0,\Omega_h}\leq C\|V^\ell\|_{0,\Omega},\quad\forall V\in L^2(\Omega_h); \tag{3.7}$$
$$c|V^\ell|_{1,\Omega}\leq|V|_{1,\Omega_h}\leq C|V^\ell|_{1,\Omega},\quad\forall V\in H^1(\Omega_h); \tag{3.8}$$
$$c\|W^\ell\|_{0,\Gamma}\leq\|W\|_{0,\Gamma_h}\leq C\|W^\ell\|_{0,\Gamma},\quad\forall V\in L^2(\Gamma_h); \tag{3.9}$$
$$c|W^\ell|_{1,\Gamma}\leq|W|_{1,\Gamma_h}\leq C|W^\ell|_{1,\Gamma},\quad\forall V\in H^1(\Gamma_h). \tag{3.10}$$

Lemma 3.3 (Geometric error of lifting)**.** *There exists $C>0$, depending on Γ and on the shape*

regularity of the mesh (see [35]*) such that for all* $u,\varphi\in H^1(\Omega)$ *and* $v,\psi\in H^1(\Gamma)$*:*

$$\left|\int_\Omega \nabla u\cdot\nabla\varphi-\int_{\Omega_h}\nabla u^{-\ell}\cdot\nabla\varphi^{-\ell}\right|\leq Ch|u|_{1,\Omega_B^\ell}|\varphi|_{1,\Omega_B^\ell};\tag{3.11}$$

$$\left|\int_\Omega u\varphi-\int_{\Omega_h}u^{-\ell}\varphi^{-\ell}\right|\leq Ch\|u\|_{0,\Omega_B^\ell}\|\varphi\|_{0,\Omega_B^\ell};\tag{3.12}$$

$$\left|\int_\Gamma \nabla_\Gamma v\cdot\nabla_\Gamma\psi-\int_{\Gamma_h}\nabla_{\Gamma_h}v^{-\ell}\cdot\nabla_{\Gamma_h}\psi^{-\ell}\right|\leq Ch^2|v|_{1,\Gamma}|\psi|_{1,\Gamma};\tag{3.13}$$

$$\left|\int_\Gamma v\psi-\int_{\Gamma_h}v^{-\ell}\psi^{-\ell}\right|\leq Ch^2\|v\|_{0,\Gamma}\|\psi\|_{0,\Gamma}.\tag{3.14}$$

Lemma 3.4 (Geometric error of the Stein extension [35])**.** *There exist* $C>0$ *depending on* Ω *and the shape regularity of the mesh such that*

$$\|\tilde{u}-u^{-\ell}\|_{0,\Omega_h}\leq Ch^2\|u\|_{2+\frac{1}{4},\Omega},\quad\forall\, u\in H^{2+\frac{1}{4}}(\Omega);\tag{3.15}$$

$$|\tilde{u}-u^{-\ell}|_{1,\Omega_h}\leq Ch^{3/2}\|u\|_{2,\Omega}+Ch\|u\|_{2+\frac{3}{4},\Omega},\quad\forall\, u\in H^{2+\frac{3}{4}}(\Omega),\tag{3.16}$$

where $\tilde{u}$ *is the Stein extension of* u *(see Theorem* A.3*).*

Even if a full proof of Lemma 3.4 can be found in [35], estimates (3.15)-(3.16) are heuristically justified as follows. In (3.16), the superconvergence of the term $\|u\|_{2,\Omega}$ of order $\frac{3}{2}$ is due to the pointwise error $\tilde{u}(\boldsymbol{x})-u^{-\ell}(\boldsymbol{x})$ vanishing for any $\boldsymbol{x}\in\Omega_h\setminus\Omega_B$, where Ω_B is the discrete narrow band defined in Section 3.1. In both estimates, the extra regularity in the terms $\|u\|_{2+\frac{1}{4},\Omega}$ and $\|u\|_{2+\frac{3}{4},\Omega}$ serves to provide sufficient Hölder continuity to estimate the aforementioned pointwise error in Ω_B.

3.3 Virtual element spaces and operators

Here, we recall from [2] all the definitions of the discrete spaces and operators required in the BS-VEM and their basic approximation error estimates. Throughout this Section let $E\in\mathcal{E}_h$ be any 3D element and $F\in\mathcal{F}_h$ be any face.

3.3.1 Construction of the discrete function spaces

The starting point is the following *boundary space* on faces:

$$\mathbb{B}(\partial F):=\left\{v\in\mathcal{C}^0(\partial F)\,\middle|\,v_{|e}\in\mathbb{P}_1(e),\,\forall e\in\text{ edges}(F)\right\},\tag{3.17}$$

then the *preliminary space* on faces is defined by

$$\widetilde{\mathbb{V}}(F):=\left\{v\in H^1(F)\,\middle|\,v_{|\partial F}\in\mathbb{B}(\partial F)\ \wedge\ \Delta v\in\mathbb{P}_1(F)\right\}.\tag{3.18}$$

The H^1 *projector* on faces $\Pi_F^\nabla:\widetilde{\mathbb{V}}(F)\to\mathbb{P}_1(F)$ is defined, for any $u\in\widetilde{\mathbb{V}}(F)$, by

$$\int_F\nabla\left(v-\Pi_F^\nabla v\right)\cdot\nabla p=0,\quad\forall p\in\mathbb{P}_1(F)\ \wedge\ \int_{\partial F}\left(v-\Pi_F^\nabla v\right)=0.\tag{3.19}$$

The *enhanced space* on faces is defined by

$$\mathbb{V}(F) := \left\{ v \in \widetilde{\mathbb{V}}(F) \middle| \int_F \left(v - \Pi_F^\nabla v \right) p = 0, \ \forall\ p \in \mathbb{P}_1(F) \right\}. \tag{3.20}$$

We can now start the construction of the 3D spaces. The *boundary space* on polyhedra is defined by[†]

$$\mathbb{B}(\partial E) := \left\{ u \in \mathcal{C}^0(\partial E) \middle| u_{|F} \in \mathbb{V}(F), \ \forall F \in \text{ faces}(E) \right\}. \tag{3.21}$$

After that, the construction continues exactly as in the 2D case addressed above. The preliminary space on polyhedra is defined by

$$\widetilde{\mathbb{V}}(E) := \left\{ u \in H^1(E) \middle| u_{|\partial E} \in \mathbb{B}(\partial E) \ \wedge \ \Delta u \in \mathbb{P}_1(E) \right\}. \tag{3.22}$$

The H^1 *projector* on polyhedra $\Pi_E^\nabla : \widetilde{\mathbb{V}}(E) \to \mathbb{P}_1(E)$ is defined, for any $u \in \mathbb{V}(E)$, by

$$\int_E \nabla \left(u - \Pi_E^\nabla u \right) \cdot \nabla q = 0, \quad \forall q \in \mathbb{P}_1(E) \ \wedge \ \int_{\partial E} \left(v - \Pi_E^\nabla v \right) = 0. \tag{3.23}$$

The *enhanced space* on polyhedra is finally defined by

$$\mathbb{V}(E) := \left\{ u \in \widetilde{\mathbb{V}}(E) \middle| \int_E \left(u - \Pi_E^\nabla u \right) p = 0, \ \forall\ p \in \mathbb{P}_1(E) \right\}. \tag{3.24}$$

From elliptic regularity, it holds that $\mathbb{V}(F) \subset H^{\frac{3}{2}+\varepsilon}(F)$ and $\mathbb{V}(E) \subset H^{1+\varepsilon}(E)$ for $\varepsilon > 0$ sufficiently small depending on F and E, as opposed to the tetrahedral FEM case where the discrete function spaces are piecewise analytic. This lack of regularity in the discrete function spaces constitutes an additional challenge in the analysis of nonlinearities and further motivates our line of proof. The L^2 *projectors* $\Pi_F^0 : \mathbb{V}(F) \to \mathbb{P}_1(F)$ and $\Pi_E^0 : \mathbb{V}(E) \to \mathbb{P}_1(E)$ are defined, for any $v \in \mathbb{V}(F)$ and $u \in \mathbb{V}(E)$, as follows:

$$\int_F \left(v - \Pi_F^0 v \right) p = 0, \quad \forall\ p \in \mathbb{P}_1(F); \tag{3.25}$$

$$\int_E \left(u - \Pi_E^0 u \right) q = 0, \quad \forall\ q \in \mathbb{P}_1(E). \tag{3.26}$$

Since this work is confined to the lowest order VEM, it holds that $\Pi_F^0 = \Pi_F^\nabla$ and $\Pi_E^0 = \Pi_E^\nabla$, see [2], but we still need the definitions (3.25)-(3.26). As proven in [2], the vertex-wise values constitute a unisolvent set of degrees of freedom (DOF) in $\mathbb{V}(F)$ and $\mathbb{V}(E)$, defined as follows[‡]:

$$\text{dof}(v) = \{ v(P) | P \in \text{ vertexes}(F) \}, \quad \forall\ v \in \mathbb{V}(F); \tag{3.27}$$

$$\text{dof}(u) = \{ u(P) | P \in \text{ vertexes}(E) \}, \quad \forall\ u \in \mathbb{V}(E). \tag{3.28}$$

[†]From elliptic regularity and Sobolev embeddings we have that $\mathbb{V}(F) \subset H^{\frac{3}{2}+\varepsilon}(F) \subset H^{1+\varepsilon}(F) \hookrightarrow \mathcal{C}^0(F)$, which implies that the definition of $\mathbb{B}(\partial E)$ in (3.21) is well-posed.

[‡]In higher order VEM spaces, which are outside the scope of this study, the DOFs are not only of pointwise type.

We define global VEM spaces by matching the DOFs across elements. To this end, let $\mathbb{S}_\Gamma$ be the 1-skeleton of Γ_h and $\mathbb{S}_\Omega$ be the 2-skeleton of Ω_h, defined respectively by

$$\mathbb{S}_\Gamma := \bigcup_{F\in\mathcal{F}_h} \partial F, \quad \text{and} \quad \mathbb{S}_\Omega := \bigcup_{E\in\mathcal{E}_h} \partial E. \tag{3.29}$$

The global spaces $\mathbb{V}_\Gamma$ and $\mathbb{V}_\Omega$ are then defined as

$$\mathbb{V}_\Gamma = \left\{ v\in H^1(\Gamma_h) \middle| v_{|\mathbb{S}_\Gamma}\in\mathcal{C}^0(\mathbb{S}_\Gamma) \ \wedge \ v_{|F}\in\mathbb{V}(F),\ \forall F\in\mathcal{F}_h \right\}; \tag{3.30}$$

$$\mathbb{V}_\Omega = \left\{ u\in H^1(\Omega_h) \middle| u_{|\mathbb{S}_\Omega}\in\mathcal{C}^0(\mathbb{S}_\Omega) \ \wedge \ u_{|E}\in\mathbb{V}(E),\ \forall E\in\mathcal{E}_h \right\}. \tag{3.31}$$

With the notation introduced in Section 3.1, the Lagrangian bases $\{\psi_i\}_{i=1}^M \subset \mathbb{V}_\Gamma$ and $\{\varphi_i\}_{i=1}^N \subset \mathbb{V}_\Omega$ are uniquely defined by $\psi_i(\boldsymbol{x}_j)=\delta_{ij}$ for all $i,j=1,\cdots,M$ and $\varphi_k(\boldsymbol{x}_l)=\delta_{kl}$ for all $k,l=1,\cdots,N$.

3.3.2 Interpolation and projection

The following definition provides a compact notation when summing over all elements, while avoiding functions that are multiply defined on the junction between elements.

Definition 3.2 (Broken Hilbert norms)**.** Given $s\in\{1,2\}$ and two collections of functions $v=\{v_F\in H^s(F)|F\in\mathcal{F}_h\}$ and $u=\{u_E\in H^s(E)|E\in\mathcal{E}_h\}$, we define the broken Hilbert seminorms of order s as follows:

$$|v|_{s,\Gamma_h,b} := \left(\sum_{F\in\mathcal{F}_h} |v_F|_{s,F}^2 \right)^{\frac{1}{2}} \quad \text{and} \quad |u|_{s,\Omega_h,b} := \left(\sum_{E\in\mathcal{E}_h} |u_E|_{s,E}^2 \right)^{\frac{1}{2}},$$

The following result provides optimal error estimates for the piecewise polynomial projection of piecewise H^1 functions on polytopal meshes.

Proposition 3.1 (Projection error on polynomials [2])**.** For $s\in\{1,2\}$, given two collections of functions $v=\{v_F\in H^s(F)|F\in\mathcal{F}_h\}$ and $u=\{u_E\in H^s(E)|E\in\mathcal{E}_h\}$, there exist $v_\pi\in\prod_{F\in\mathcal{F}_h}\mathbb{P}_1(F)$ and $u_\pi\in\prod_{E\in\mathcal{E}_h}\mathbb{P}_1(E)$ such that

$$\|v-v_\pi\|_{0,\Gamma_h} + h|v-v_\pi|_{1,\Gamma_h,b} \le Ch^s|v|_{s,\Gamma_h,b}; \tag{3.32}$$

$$\|u-u_\pi\|_{0,\Omega_h} + h|u-u_\pi|_{1,\Omega_h,b} \le Ch^s|u|_{s,\Omega_h,b}, \tag{3.33}$$

where C is a constant that depends only on the shape regularity of the mesh.

We now analyse the properties of VEM interpolants and projectors. Let $I_F: H^2(F)\to\mathbb{V}(F)$ and $I_E: H^2(E)\to\mathbb{V}(E)$ be the element-wise VEM interpolant operators. Let $I_\Gamma: \Pi_{F\in\mathcal{F}_h}H^2(F)\to\Pi_{F\in\mathcal{F}_h}\mathbb{V}(F)$ and $I_\Omega: \Pi_{E\in\mathcal{E}_h}H^2(E)\to\Pi_{E\in\mathcal{E}_h}\mathbb{V}(E)$ be the corresponding (possibly discontinuous) global interpolant operators. Let $\Pi^0_\Gamma: \Pi_{F\in\mathcal{F}_h}\mathbb{V}(F)\to\Pi_{F\in\mathcal{F}_h}\mathbb{P}_1(F)$ and $\Pi^0_\Omega: \Pi_{E\in\mathcal{E}_h}\mathbb{V}(E)\to\Pi_{E\in\mathcal{E}_h}\mathbb{P}_1(E)$ be the discontinuous global projection operators that correspond to the local projector Π^0_F and Π^0_E defined in (3.25)-(3.26).

Proposition 3.2 (Stability of VEM L^2 projectors)**.** The L^2 projection operators Π_E^0 and Π_F^0 fulfil, for any $v \in \mathbb{V}(F)$ and $u \in \mathbb{V}(E)$, the following stability bounds

$$\|\Pi_F^0 v\|_{0,F} \leq \|v\|_{0,F} \quad \text{and} \quad |\Pi_F^0 v|_{1,F} \leq |v|_{1,F}; \tag{3.34}$$

$$\|\Pi_E^0 u\|_{0,E} \leq \|u\|_{0,E} \quad \text{and} \quad |\Pi_E^0 u|_{1,E} \leq |u|_{1,E}. \tag{3.35}$$

Proof. The bounds on the left of (3.34)-(3.35) follow by testing (3.25)-(3.26) with $p = \Pi_F^0 v$ and $q = \Pi_E^0 u$ and using the Cauchy-Schwarz inequality. The bounds on the right of (3.34)-(3.35) are obtained by testing (3.19) and (3.23) by $v = \Pi_F^\nabla v$ and $u = \Pi_E^\nabla u$, using the Cauchy-Schwarz inequality and then noting that $\Pi_F^\nabla = \Pi_F^0$ and $\Pi_E^\nabla = \Pi_E^0$ as discussed above. □

Proposition 3.3 (VEM interpolation error [2])**.** Given two collections of functions $v = \{v_F \in H^2(F) \,|\, F \in \mathcal{F}_h\}$ and $u = \{u_E \in H^2(E) \,|\, E \in \mathcal{E}_h\}$, then it holds that

$$\|v - I_\Gamma(v)\|_{0,\Gamma_h} + h|v - I_\Gamma(v)|_{1,\Gamma_h,b} \leq Ch^2 |v|_{2,\Gamma_h,b}; \tag{3.36}$$

$$\|u - I_\Omega(u)\|_{0,\Omega_h} + h|u - I_\Omega(u)|_{1,\Omega_h,b} \leq Ch^2 |u|_{2,\Omega_h,b}, \tag{3.37}$$

respectively, where $C > 0$ depends only on the shape regularity of the mesh.

As opposed to Proposition 3.1, Proposition 3.3 does not include the case when the Hilbert regularity of the interpolated function is $s = 1$. This is a consequence of the interpolant operators I_Ω and I_Γ being well-defined if and only if the interpolated function is continuous, which in turn requires $v \in H^{1+\varepsilon}$ in two dimensions (on faces) and $u \in H^{\frac{3}{2}+\varepsilon}$ in three dimensions (on polyhedra), for any $\varepsilon > 0$. Notably, in three dimensions *not even* $\mathbb{V}_\Omega$ *functions themselves* are regular enough to be interpolated, an issue that is easily overcome by noting that, on $\mathbb{V}_\Omega$ itself, the interpolant acts as the identity. Another dissimilarity from the L^2 projectors is that VEM interpolants I_Γ and I_Ω are not stable in L^2, i.e. they do not fulfil analogous bounds as (3.34)-(3.35). Instead, they fulfil $\mathcal{O}(h^2)$-perturbed stability estimates thanks to (3.36)-(3.37) combined with the triangle inequality, but only if the interpolated function is H^2. In short, VEM interpolants are only *conditionally stable*. Notably, on the class of *Lipschitz-transformed VEM functions*, which is not even contained in H^2, VEM interpolants exhibit a stable behaviour as illustrated in the following Lemma.

Lemma 3.5 (Stability of VEM interpolants on Lipschitz-transformed VEM spaces)**.** *Given* $\mu \in \mathbb{N}$ *and given two Lipschitz functions* $s : (\mathbb{V}_\Gamma)^\mu \to \mathbb{R}$ *and* $r : (\mathbb{V}_\Omega)^\mu \to \mathbb{R}$*, there exists* $C > 0$ *depending on the shape regularity of* Ω_h*, on the Lipschitz constants of* s*,* r *and on the values* $s(\mathbf{0})$*,* $r(\mathbf{0})$ *such that, for all* $V_1, \cdots, V_\mu \in \mathbb{V}_\Gamma$*,* $v_1, \cdots, v_\mu \in \mathcal{C}^0(\Gamma_h)$*,* $U_1, \cdots, U_\mu \in \mathbb{V}_\Omega$*, and* $u_1, \cdots, u_\mu \in$

$\mathcal{C}^0(\Omega_h)$

$$\left\|I_\Gamma(s(V_1,\cdots,V_\mu)-s(v_1,\cdots,v_\mu))\right\|^2_{0,\Gamma_h}\leq C\sum_{i=1}^{\mu}\|V_i-I_\Gamma v_i\|^2_{0,\Gamma_h}; \tag{3.38}$$

$$\left\|I_\Omega(r(U_1,\cdots,U_\mu)-r(u_1,\cdots,u_\mu))\right\|^2_{0,\Omega_h}\leq C\sum_{i=1}^{\mu}\|U_i-I_\Omega u_i\|^2_{0,\Omega_h}; \tag{3.39}$$

$$\left\|I_\Gamma(s(V_1,\cdots,V_\mu))\right\|^2_{0,\Gamma_h}\leq C\left(\sum_{i=1}^{\mu}\|V_i\|^2_{0,\Gamma_h}+1\right); \tag{3.40}$$

$$\left\|I_\Omega(r(U_1,\cdots,U_\mu))\right\|^2_{0,\Omega_h}\leq C\left(\sum_{i=1}^{\mu}\|U_i\|^2_{0,\Omega_h}+1\right). \tag{3.41}$$

Proof. A proof of (3.38)-(3.39) is given in [40, Lemma 5] for $\mu=1$, the extension to $\mu\in\mathbb{N}$ is trivial. The stability estimates (3.40)-(3.41) follow from (3.38)-(3.39), respectively, by choosing $v_i=0$ and $u_i=0$ for all $i=1,\cdots,\mu$ and using the triangle inequality. □

3.3.3 Discrete bilinear forms

To provide a discrete formulation of problem (2.2), we consider the discrete bilinear forms $m_F:\mathbb{V}(F)\times\mathbb{V}(F)\to\mathbb{R}$, $a_F:\mathbb{V}(F)\times\mathbb{V}(F)\to\mathbb{R}$, $m_E:\mathbb{V}(E)\times\mathbb{V}(E)\to\mathbb{R}$ and $a_E:\mathbb{V}(E)\times\mathbb{V}(E)\to\mathbb{R}$ defined as follows:

$$m_F(v,w)=\int_F\Pi^0_F v\Pi^0_F w+h_F^2\left\langle\mathrm{dof}\left(v-\Pi^0_F v\right),\mathrm{dof}\left(w-\Pi^0_F w\right)\right\rangle; \tag{3.42}$$

$$a_F(v,w)=\int_F\nabla\Pi^\nabla_F v\cdot\nabla\Pi^\nabla_F w+\left\langle\mathrm{dof}\left(v-\Pi^\nabla_F v\right),\mathrm{dof}\left(w-\Pi^\nabla_F w\right)\right\rangle; \tag{3.43}$$

$$m_E(u,z)=\int_E\Pi^0_E u\Pi^0_E z+h_E^3\left\langle\mathrm{dof}\left(u-\Pi^0_E u\right),\mathrm{dof}\left(z-\Pi^0_E z\right)\right\rangle; \tag{3.44}$$

$$a_E(u,z)=\int_E\nabla\Pi^\nabla_E u\cdot\nabla\Pi^\nabla_E z+h_E\left\langle\mathrm{dof}\left(u-\Pi^\nabla_E u\right),\mathrm{dof}\left(z-\Pi^\nabla_E z\right)\right\rangle, \tag{3.45}$$

for all $v,w\in\mathbb{V}(F)$ and $u,z\in\mathbb{V}(E)$, where $\langle\cdot,\cdot\rangle$ denotes the Euclidean inner product. Let $m_h^\Gamma:\mathbb{V}_\Gamma\times\mathbb{V}_\Gamma\to\mathbb{R}$, $a_h^\Gamma:\mathbb{V}_\Gamma\times\mathbb{V}_\Gamma\to\mathbb{R}$, $m_h^\Omega:\mathbb{V}_\Omega\times\mathbb{V}_\Omega\to\mathbb{R}$, and $a_h^\Omega:\mathbb{V}_\Omega\times\mathbb{V}_\Omega\to\mathbb{R}$ be the corresponding global forms. Let $A_\Gamma=(a^\Gamma_{k,l})\in\mathbb{R}^{M\times M}$ and $A_\Omega=(a^\Omega_{i,j})\in\mathbb{R}^{N\times N}$ be the stiffness matrices, let $M_\Gamma=(m^\Gamma_{k,l})\in\mathbb{R}^{M\times M}$ and $M_\Omega=(m^\Omega_{i,j})\in\mathbb{R}^{N\times N}$ be the mass matrices, and let $K_\Gamma=(\kappa^\Gamma_{k,l})\in\mathbb{R}^{M\times M}$ and $K_\Omega=(\kappa^\Omega_{i,j})\in\mathbb{R}^{N\times N}$ be the *consistency matrices* defined as follows:

$$a^\Gamma_{k,l}:=a^\Gamma_h(\psi_k,\psi_l),\quad m^\Gamma_{k,l}:=m^\Gamma_h(\psi_k,\psi_l),\quad \kappa^\Gamma_{k,l}:=\int_{\Gamma_h}\Pi^0_\Gamma\psi_k\Pi^0_\Gamma\psi_l,\quad k,l=1,\cdots,M; \tag{3.46}$$

$$a^\Omega_{i,j}:=a^\Omega_h(\varphi_i,\varphi_j),\quad m^\Omega_{i,j}:=m^\Omega_h(\varphi_i,\varphi_j),\quad \kappa^\Omega_{i,j}:=\int_{\Omega_h}\Pi^0_\Omega\varphi_i\Pi^0_\Omega\varphi_j,\quad i,j=1,\cdots,N. \tag{3.47}$$

Proposition 3.4 (Stability and consistency [2])**.** The bilinear forms m_F, a_F, m_E, and a_E are consistent, i.e. for all $v\in\mathbb{V}(F)$ and $u\in\mathbb{V}(E)$

$$a_F(v,p)=\int_F \nabla v\cdot\nabla p;\quad\text{and}\quad m_F(v,p)=\int_F vp,\quad \forall p\in\mathbb{P}_1(F); \tag{3.48}$$

$$a_E(u,q)=\int_E \nabla u\cdot\nabla q;\quad\text{and}\quad m_E(u,q)=\int_E uq,\quad \forall q\in\mathbb{P}_1(E). \tag{3.49}$$

Furthermore, the bilinear forms m_F, a_F, m_E, and a_E are stable, meaning that there exist two constants $0<c<C$ depending on the shape regularity of the mesh such that, for all $v\in\mathbb{V}(F)$ and $u\in\mathbb{V}(E)$

$$c|v|^2_{1,F}\le a_F(v,v)\le C|v|^2_{1,F}\quad\text{and}\quad c\|v\|^2_{0,F}\le m_F(v,v)\le C\|v\|^2_{0,F}; \tag{3.50}$$

$$c|u|^2_{1,E}\le a_E(u,u)\le C|u|^2_{1,E}\quad\text{and}\quad c\|u\|^2_{0,E}\le m_E(u,u)\le C\|u\|^2_{0,E}. \tag{3.51}$$

3.4 The spatially discrete formulation

We are now ready to introduce the *bulk-surface virtual element discretisation* of the weak BS-RDS (2.2), which is: find $U\in H^1([0,T];\mathbb{V}_\Omega)$, $V\in H^1([0,T];\mathbb{V}_\Gamma)$ such that

$$\begin{cases} m_h^\Omega\left(\dot U,\varphi\right)+d_u a_h^\Omega\Big(U,\varphi\Big)=\displaystyle\int_{\Omega_h} I_\Omega(q(U))\Pi^0\varphi+\int_{\Gamma_h} I_\Gamma(s(U,V))\Pi^0\varphi;\\ m_h^\Gamma\left(\dot V,\psi\right)+d_v a_h^\Gamma\Big(V,\psi\Big)=\displaystyle\int_{\Gamma_h} I_\Gamma(r(U,V)-s(U,V))\Pi^0\psi, \end{cases} \tag{3.52}$$

for all $\varphi\in L^2([0,T];\mathbb{V}_\Omega)$, $\psi\in L^2([0,T];\mathbb{V}_\Gamma)$. The discrete initial conditions are prescribed as the VEM interpolants of the exact initial conditions, that is

$$U_0=I_\Omega(u_0),\quad\text{and}\quad V_0=I_\Gamma(v_0), \tag{3.53}$$

which are well-defined thanks to the regularity of u_0 and v_0, see Assumption 1.

Remark 3.1 (Formulation of the method)**.** The treatment of the right-hand side in the method (3.52) is an adaptation of the approach proposed in [1] and is specifically devised to ensure at once

- computability;
- the method only relies on nodal values (degrees of freedom) regardless of the functional form of the nonlinear functions q,r,s, thereby avoiding costly quadratures on general polyhedra and polygons;
- optimal convergence. In fact, thanks to the *stability of VEM interpolants on Lipschitz-transformed VEM spaces* (Lemma 3.5), we will be able to show that the interpolants appearing in the nonlinearities of the discrete formulation (3.52) are quadratically accurate in the meshsize even if the $\mathbb{V}(\Omega)$ and $\mathbb{V}(\Gamma)$ functions are not H^2 on non-convex elements.

Remark 3.2 (Extension to higher order)**.** A consequence of Lemma 3.1 is that, to achieve higher order spatial convergence, it is necessary to adopt curved elements. The main challenge in devising a higher order BS-VEM resides in the definition of the spaces $\mathbb{V}_\Omega$ and $\mathbb{V}_\Gamma$ themselves. For the bulk space $\mathbb{V}_\Omega$, the problem was successfully addressed in different contexts., i.e. in 2D [13] and 3D for a Darcy problem in mixed form [28]. For 3D differential operators in standard form, to the best of our knowledge, the problem is open. For the surface space $\mathbb{V}_\Gamma$, a parametric VEM relying on explicit knowledge of local charts was proposed in [6]. An additional challenge is that we require $\mathbb{V}_\Gamma$ to be the trace of $\mathbb{V}_\Omega$, hence (i) the two spaces cannot be constructed independently from each other and (ii) $\mathbb{V}_\Omega$ must be constructed in such a way that in its trace $\mathbb{V}_\Gamma$, the Laplace-Beltrami operator is computable.

4 Stability and convergence analysis

By adapting the techniques used in [34] to the present 3D context, we prove stability estimates for the spatially discrete problem (3.52) in the following Lemma.

Lemma 4.1 (Stability estimates for the spatially discrete BS-RDS (3.52))**.** *There exists $C>0$ depending on Ω, on the kinetics q,r,s, and on the shape regularity of the mesh such that*

$$\begin{aligned}&\sup_{t\in[0,T]}\left(\|U\|^2_{0,\Omega_h}+\|V\|^2_{0,\Gamma_h}\right)+\int_0^T\left(|U|^2_{1,\Omega_h}+|V|^2_{1,\Gamma_h}\right)\\ \le& C\left(1+\|U_0\|^2_{0,\Omega_h}+\|V_0\|^2_{0,\Gamma_h}\right)\exp(CT);\end{aligned}\tag{4.1}$$

$$\begin{aligned}&\sup_{t\in[0,T]}\left(|U|^2_{1,\Omega_h}+|V|^2_{1,\Gamma_h}\right)+\int_0^T\left(\|\dot U\|^2_{0,\Omega_h}+\|\dot V\|^2_{0,\Gamma_h}\right)\\ \le& C\left(1+\|U_0\|^2_{1,\Omega_h}+\|V_0\|^2_{1,\Gamma_h}\right)\exp(CT).\end{aligned}\tag{4.2}$$

Proof. The proof relies on standard energy techniques. By (i) choosing $\varphi=U$ and $\psi=V$ in (3.52) and summing over the equations, (ii) estimating the nonlinearities with (3.40)-(3.41) and (iii) using Proposition 3.2, Cauchy-Schwarz and Young's inequalities we have

$$\begin{aligned}&\frac{1}{2}\frac{\mathrm{d}}{\mathrm{d}t}\left(m^\Omega_h(U,U)+m^\Gamma_h(V,V)\right)+d_u a^\Omega_h(U,U)+d_v a^\Gamma_h(V,V)\\ \le& C\left(1+\|U\|^2_{0,\Omega_h}+\|V\|^2_{0,\Gamma_h}\right)+c\|U_{|\Gamma_h}\|^2_{0,\Gamma_h},\end{aligned}\tag{4.3}$$

with $c>0$ being arbitrarily small, thanks to Young's inequality. By applying the trace inequality (A.3) to the rightmost term in (4.3) and then using (3.8), (3.50)-(3.51), we can

choose c such that

$$\begin{aligned}&\frac{1}{2}\frac{\mathrm{d}}{\mathrm{d}t}\Big(m_h^\Omega(U,U)+m_h^\Gamma(V,V)\Big)+d_u a_h^\Omega(U,U)+d_v a_h^\Gamma(V,V)\\ \le& C\Big(1+\|U\|_{0,\Omega_h}^2+\|V\|_{0,\Gamma_h}^2\Big)+\frac{d_u}{2}a_h^\Omega(U,U).\end{aligned}\tag{4.4}$$

By using (3.51)-(3.50) into (4.4) we have

$$\begin{aligned}\frac{1}{2}\frac{\mathrm{d}}{\mathrm{d}t}\Big(m_h^\Omega(U,U)+m_h^\Gamma(V,V)\Big)\le& C\Big(m_h^\Omega(U,U)+m_h^\Gamma(V,V)\Big)\\ &+C-\frac{d_u}{2}a_h^\Omega(U,U)-d_v a_h^\Gamma(V,V).\end{aligned}\tag{4.5}$$

An application of Grönwall's lemma to (4.5) yields

$$\begin{aligned}&\sup_{t\in[0,T]}\Big(m_h^\Omega(U,U)+m_h^\Gamma(V,V)\Big)\\ \le&\Big(1+m_h^\Omega(U_0,U_0)+m_h^\Gamma(V_0,V_0)\Big)\exp(CT)\\ &-1-\int_0^T\Big(\frac{d_u}{2}a_h^\Omega(U,U)+d_v a_h^\Gamma(V,V)\Big)\exp\{C(T-t)\}\mathrm{d}t,\end{aligned}\tag{4.6}$$

which yields (4.1) after using (3.8). Similarly, by choosing $\varphi=\dot{U}$ and $\psi=\dot{V}$ in (3.52) and summing over the equations we have

$$\begin{aligned}&m_h^\Omega(\dot{U},\dot{U})+m_h^\Gamma(\dot{V},\dot{V})+\frac{1}{2}\frac{\mathrm{d}}{\mathrm{d}t}\Big(d_u a_h^\Omega(U,U)+d_v a_h^\Gamma(V,V)\Big)\\ \le& C\Big(1+\|U\|_{0,\Omega_h}^2+\|V\|_{0,\Gamma_h}^2\Big)+Ca_h^\Omega(U,U)+\frac{1}{2}\Big(m_h^\Omega(\dot{U},\dot{U})+m_h^\Gamma(\dot{V},\dot{V})\Big),\end{aligned}\tag{4.7}$$

where we have exploited the Lipschitz continuity of q,r,s, Young's inequality and (3.50)-(3.51). From (4.7) we get

$$\begin{aligned}&\frac{1}{2}\Big(m_h^\Omega(\dot{U},\dot{U})+m_h^\Gamma(\dot{V},\dot{V})\Big)+\frac{1}{2}\frac{\mathrm{d}}{\mathrm{d}t}\Big(d_u a_h^\Omega(U,U)+d_v a_h^\Gamma(V,V)\Big)\\ \le& C\Big(a_h^\Omega(U,U)+a_h^\Gamma(V,V)\Big)+C\Big(1+\|U\|_{0,\Omega_h}^2+\|V\|_{0,\Gamma_h}^2\Big).\end{aligned}\tag{4.8}$$

By applying Grönwall's lemma and then using (3.50)-(3.51) we obtain (4.2). □

To derive error estimates for the spatially discrete solution (3.52) we need suitable bulk- and surface-Ritz projections that we had introduced in [35], where the reader is referred for details on the proofs.

Definition 4.1 (Surface-Ritz projection)**.** The *surface-Ritz projection* of a function $v\in H^1(\Gamma)$ is the unique function $\mathcal{R}v\in\mathbb{V}_\Gamma$ such that

$$a_h^\Gamma(\mathcal{R}v,\psi)=\int_\Gamma\nabla_\Gamma v\cdot\nabla_\Gamma\psi^\ell\quad\forall\psi\in\mathbb{V}_\Gamma,\quad\text{and}\quad\int_{\Gamma_h}\mathcal{R}v=\int_\Gamma v.\tag{4.9}$$

Theorem 4.1 (Error bound for the surface-Ritz projection)**.** *There exists $C>0$ depending only on Γ such that, for any $v\in H^2(\Gamma)$, the surface-Ritz projection $\mathcal{R}v$ fulfils*

$$\|v-(\mathcal{R}v)^\ell\|_{0,\Gamma}+h\|v-(\mathcal{R}v)^\ell\|_{1,\Gamma}\leq Ch^2\|v\|_{2,\Gamma}. \tag{4.10}$$

Proof. The proposed surface-Ritz projection is a combination of the Ritz projections for the SFEM [32] and VEM [56], respectively. A complete proof for the H^1 estimate can be found in [38], while the L^2 estimate follows from the H^1 estimate combined with a standard Aubin-Nitsche argument. □

Definition 4.2 (Bulk-Ritz projection)**.** The *bulk-Ritz projection* of a function $u\in H^1(\Omega)$ is the unique function $\mathcal{R}u\in\mathbb{V}_\Omega$ such that

$$a_h^\Omega(\mathcal{R}u,\psi)=\int_\Omega\nabla u\cdot\nabla\psi^\ell\quad\forall\,\psi\in\mathbb{V}_\Omega,\quad\text{and}\quad\mathcal{R}u_{|\Gamma_h}=I_\Gamma(u^{-\ell}). \tag{4.11}$$

Theorem 4.2 (Error bounds for the bulk-Ritz projection)**.** *If the surface Γ is $\mathcal{C}^3$, then for any $u\in H^{2+\frac{3}{4}}(\Omega)$ with $\mathrm{Tr}(u)\in H^2(\Gamma)$ and for h sufficiently small, it holds that*

$$\|u-(\mathcal{R}u)^\ell\|_{0,\Omega}+h|u-(\mathcal{R}u)^\ell|_{1,\Omega}\leq Ch^2\left(\|u\|_{2,\Omega}+\|u\|_{2+\frac{3}{4},\Omega}\right), \tag{4.12}$$

$$\|u-(\mathcal{R}u)^\ell\|_{0,\Gamma}+h|u-(\mathcal{R}u)^\ell|_{1,\Gamma}\leq Ch^2\|u\|_{2,\Gamma}, \tag{4.13}$$

with C depending on Ω and on the shape regularity of the mesh (see [35]*). In* (4.12)*, the term in $H^{2+\frac{3}{4}}(\Omega)$ norm arises only in the simultaneous presence of a curved surface Γ and non-tetrahedral bulk elements that touch Γ.*

Proof. The proof is analogous to the proofs of [34, Theorems 4 and 5], except for the exponent $2+\frac{3}{4}$ in (4.12) instead of the exponent $2+\frac{1}{4}$ appearing in its 2D counterpart, as a consequence of (3.15)-(3.16). □

The following theorem shows optimal quadratic convergence in the Bochner norm $L^2([0,T];L^2(\Omega)\times L^2(\Gamma))$ for the spatially discrete BS-RDS (3.52). The theorem is the 3D counterpart of [34, Theorem 6] and contains substantial modifications due to the different spatial discretisation of the surface equations in 3D.

Theorem 4.3 (Convergence of the BS-VEM)**.** *Under Conjecture* 1*, the solution (U,V) of* (3.52) *fulfils the following error estimate*

$$\|u-U^\ell\|_{L^2([0,T];L^2(\Omega))}+\|v-V^\ell\|_{L^2([0,T];L^2(\Gamma))}\leq Ch^2, \tag{4.14}$$

where C depends on Ω, the diffusion coefficient d_u, the functions q,r,s, the shape regularity of the mesh, the final time T and on the following norms:

- $\|(u,\dot{u})\|_{L^2([0,T];H^2(\Omega))}$, $\|(v,\dot{v},\mathrm{Tr}(u),\mathrm{Tr}(\dot{u}))\|_{L^2([0,T];H^2(\Gamma))}$ *in any case;*

- $\|(u,\dot{u})\|_{L^2([0,T];H^{2+\frac{3}{4}}(\Omega))}$ *only in the simultaneous presence of a curved surface* Γ *and non-tetrahedral bulk elements that touch* Γ.

Proof. We split the error in terms of $\rho_u,\rho_v,\theta_u,\theta_v$ defined as follows

$$(u,v)-(U^\ell,V^\ell)=\underbrace{((u,v)-(\mathcal{R}u,\mathcal{R}v)^\ell)}_{(\rho_u,\rho_v)}+\underbrace{((\mathcal{R}u,\mathcal{R}v)-(U,V))^\ell}_{(\theta_u,\theta_v)}. \tag{4.15}$$

From (4.10), (4.12) and (4.13), since the Ritz projections commute with time derivatives, we have that

$$\|(\mathrm{Tr}(\rho_u),\mathrm{Tr}(\dot{\rho}_u),\rho_v,\dot{\rho}_v)\|_{0,\Gamma}\leq Ch^2\|(\mathrm{Tr}(u),\mathrm{Tr}(\dot{u}),v,\dot{v})\|_{2,\Gamma}; \tag{4.16}$$

$$\|(\rho_u,\dot{\rho}_u)\|_{0,\Omega}\leq Ch^2\left(\|(u,\dot{u})\|_{2,\Omega}+\|(u,\dot{u})\|_{2+\frac{3}{4},\Omega}\right). \tag{4.17}$$

We are left to estimate the norms of θ_u and θ_v. By using (2.1), (3.52), (4.11) and (4.15) we have the following error equation

$$\begin{aligned}
&m_h^\Omega\left(\dot{\theta}_u^{-\ell},\varphi\right)+d_u a_h^\Omega\left(\theta_u^{-\ell},\varphi\right)+m_h^\Gamma\left(\dot{\theta}_v^{-\ell},\psi\right)+d_v a_h^\Gamma(\theta_v^{-\ell},\psi)\\
=&m_h^\Omega\left(\dot{U},\varphi\right)-m_h^\Omega(\mathcal{R}\dot{u},\varphi)+d_u a_h^\Omega(U,\varphi)-d_u a_h^\Omega(\mathcal{R}u,\varphi)\\
&+m_h^\Gamma\left(\dot{V},\psi\right)-m_h^\Gamma(\mathcal{R}\dot{v},\psi)+d_v a_h^\Gamma(V,\psi)-d_v a_h^\Gamma(\mathcal{R}v,\psi)\\
=&\int_{\Omega_h}I_\Omega(q(U))\Pi_\Omega^0\varphi-m_h^\Omega(\mathcal{R}\dot{u},\varphi)-d_u a_h^\Omega(\mathcal{R}u,\varphi)+\int_{\Gamma_h}I_\Gamma(s(U,V))\Pi_\Gamma^0\mathrm{Tr}(\varphi)\\
&+\int_{\Gamma_h}I_\Gamma(r(U,V))\Pi_\Gamma^0\psi-m_h^\Gamma(\mathcal{R}\dot{v},\psi)-d_v a_h^\Gamma(\mathcal{R}v,\psi)-\int_{\Gamma_h}I_\Gamma(s(U,V))\Pi_\Gamma^0\psi\\
=&\underbrace{\int_\Omega\dot{u}\varphi^\ell-m_h^\Omega(\mathcal{R}\dot{u},\varphi)}_{T_1}+\underbrace{\int_{\Omega_h}I_\Omega(q(U))\Pi_\Omega^0\varphi-\int_\Omega q(u)\varphi^\ell}_{T_2}\\
&+\underbrace{\int_\Gamma\dot{v}\psi^\ell-m_h^\Gamma(\mathcal{R}\dot{v},\psi)}_{T_3}+\underbrace{\int_{\Gamma_h}I_\Gamma(r(U,V))\Pi_\Gamma^0\psi-\int_\Gamma r(u,v)\psi^\ell}_{T_4}\\
&+\underbrace{\int_{\Gamma_h}I_\Gamma(s(U,V))\Pi_\Gamma^0(\mathrm{Tr}\varphi-\psi)-\int_\Gamma(s(u,v))(\mathrm{Tr}(\varphi)-\psi)^\ell}_{T_5}.
\end{aligned}\tag{4.18}$$

We now estimate terms T_1 through T_5 on the right hand side of (4.18) in turn. For T_1 we

use (A.2) from the Appendix, (3.12) and (4.17):

$$\begin{aligned}
T_1 &= \int_\Omega (\dot{u}-(\mathcal{R}\dot{u})^\ell)\varphi^\ell + \int_\Omega (\mathcal{R}\dot{u})^\ell\varphi^\ell - \int_{\Omega_h}\mathcal{R}\dot{u}\varphi + \int_{\Omega_h}\mathcal{R}\dot{u}\varphi - m_h^\Omega(\mathcal{R}\dot{u},\varphi)\\
&\le \|\dot{u}-(\mathcal{R}\dot{u})^\ell\|_{0,\Omega}\|\varphi^\ell\|_{0,\Omega} + Ch\|(\mathcal{R}\dot{u})^\ell\|_{0,\Omega_B^\ell}\|\varphi^\ell\|_{0,\Omega_B^\ell} + \int_{\Omega_h}\mathcal{R}\dot{u}\varphi - m_h^\Omega(\mathcal{R}\dot{u},\varphi)\\
&\le \|\dot{u}-(\mathcal{R}\dot{u})^\ell\|_{0,\Omega}\|\varphi^\ell\|_{0,\Omega} + Ch^2\|(\mathcal{R}\dot{u})^\ell\|_{1,\Omega}\|\varphi^\ell\|_{1,\Omega} + \int_{\Omega_h}\mathcal{R}\dot{u}\varphi - m_h^\Omega(\mathcal{R}\dot{u},\varphi)\\
&\le Ch^2\left(\|\dot{u}\|_{2,\Omega}+\|\dot{u}\|_{2+\frac{3}{4},\Omega}\right)\|\varphi^\ell\|_{1,\Omega} + \int_{\Omega_h}\mathcal{R}\dot{u}\varphi - m_h^\Omega(\mathcal{R}\dot{u},\varphi). \qquad (4.19)
\end{aligned}$$

We estimate the last term in (4.19) using (A.2), (A.4), (3.7), (3.15), (3.33), (3.49) and (4.17):

$$\begin{aligned}
\int_{\Omega_h}\mathcal{R}\dot{u}\varphi - m_h^\Omega(\mathcal{R}\dot{u},\varphi) &= \int_{\Omega_h}(\mathcal{R}\dot{u}-\dot{\tilde{u}}_\pi)\varphi - m_h^\Omega(\mathcal{R}\dot{u}-\dot{\tilde{u}}_\pi,\varphi)\\
&\le \|\mathcal{R}\dot{u}-\dot{\tilde{u}}_\pi\|_{0,\Omega_h}\|\varphi\|_{0,\Omega_h}\\
&\le C\left(\|\dot{\rho}_u\|_{0,\Omega}+\|\dot{u}^{-\ell}-\dot{\tilde{u}}\|_{0,\Omega_h}+\|\dot{\tilde{u}}-\dot{\tilde{u}}_\pi\|_{0,\Omega_h}\right)\|\varphi^\ell\|_{0,\Omega}\\
&\le Ch^2\left(\|\dot{u}\|_{2,\Omega}+\|\dot{u}\|_{2+\frac{3}{4},\Omega}\right)\|\varphi^\ell\|_{0,\Omega}. \qquad (4.20)
\end{aligned}$$

By combining (4.19) and (4.20) we get

$$T_1 \le Ch^2\left(\|\dot{u}\|_{2,\Omega}+\|\dot{u}\|_{2+\frac{3}{4},\Omega}\right)\|\varphi^\ell\|_{1,\Omega}. \qquad (4.21)$$

We estimate T_2 by adapting the approach used in [1, Theorem 4.2]. From (A.2), (3.12), (3.15), (3.35), (3.37), (3.39) and (4.17), we have that

$$\begin{aligned}
T_2 &= \int_{\Omega_h} I_\Omega(q(U)-q(\tilde{u}))\Pi_\Omega^0\varphi + \int_{\Omega_h}(I_\Omega q(\tilde{u})-q(\tilde{u}))\Pi_\Omega^0\varphi\\
&\quad + \int_{\Omega_h}(q(\tilde{u})-q(u^{-\ell}))\Pi_\Omega^0\varphi + \int_{\Omega_h} q(u^{-\ell})\Pi_\Omega^0\varphi - \int_\Omega q(u)(\Pi_\Omega^0\varphi)^\ell\\
&\le C\|U-I_\Omega\tilde{u}\|\|\Pi_\Omega^0\varphi\|_{0,\Omega_h} + Ch^2\|q(\tilde{u})\|_{2,\Omega_h}\|\Pi_\Omega^0\varphi\|_{0,\Omega_h}\\
&\quad + Ch^2\|u\|_{2+\frac{1}{4},\Omega}\|\Pi_\Omega^0\varphi\|_{0,\Omega_h} + Ch\|q(u)\|_{0,\Omega_B^\ell}\|(\Pi_\Omega^0\varphi)^\ell\|_{0,\Omega_B^\ell}\\
&\le C(\|U-u\|_{0,\Omega_h}+\|u-\tilde{u}\|_{0,\Omega_h}+\|\tilde{u}-I_\Omega\tilde{u}\|_{0,\Omega_h})\|\varphi\|_{0,\Omega_h}\\
&\quad + Ch^2(\|\tilde{u}\|_{2,\Omega_h}+1)\|\varphi\|_{0,\Omega_h} + Ch^2\|u\|_{2+\frac{1}{4},\Omega}\|\varphi\|_{0,\Omega_h} + Ch^2(\|u\|_{1,\Omega}+1)\|\varphi^\ell\|_{1,\Omega}\\
&\le C\left(\|\theta_u\|_{0,\Omega}+h^2\|u\|_{2,\Omega}+h^2\|u\|_{2+\frac{3}{4},\Omega}\right)\|\varphi^\ell\|_{1,\Omega}. \qquad (4.22)
\end{aligned}$$

As for T_3, from (A.2), (3.9), (3.14), (3.48) and (4.16) we have that

$$\begin{aligned}
T_3 &= \int_\Gamma \dot{v}\psi^\ell - \int_{\Gamma_h}\dot{v}^{-\ell}\psi + \int_{\Gamma_h}\dot{v}^{-\ell}\psi - \int_{\Gamma_h}\mathcal{R}\dot{v}\psi + \int_{\Gamma_h}\mathcal{R}\dot{v}\psi - m_h^\Gamma(\mathcal{R}\dot{v},\psi)\\
&\le Ch^2\|\dot{v}\|_{0,\Gamma}\|\psi^\ell\|_{0,\Gamma} + C\|\dot{\rho}_v\|_{0,\Gamma}\|\psi^\ell\|_{0,\Gamma} \le Ch^2\|\dot{v}\|_{2,\Gamma}\|\psi^\ell\|_{0,\Gamma}. \qquad (4.23)
\end{aligned}$$

To estimate T_4 we proceed as in (4.22). Specifically, from (3.14), (3.34), (3.36), (3.38), and (4.16), we have that

$$T_4 \leq C\|(\theta_u,\theta_v)\|_{0,\Gamma}\|\psi^\ell\|_{0,\Gamma}+Ch^2\|(u,v)\|_{2,\Gamma}\|\psi^\ell\|_{0,\Gamma}. \tag{4.24}$$

We estimate T_5 as in (4.24) by also using (A.3):

$$\begin{aligned} T_5 &\leq C\big(\|(\theta_u,\theta_v)\|_{0,\Gamma}+Ch^2\|(u,v)\|_{2,\Gamma}\big)\|\mathrm{Tr}(\varphi^\ell)-\psi^\ell\|_{0,\Gamma} \\ &\leq C\big(\|(\theta_u,\theta_v)\|_{0,\Gamma}+Ch^2\|(u,v)\|_{2,\Gamma}\big)\big(\|\varphi^\ell\|_{1,\Omega}+\|\psi^\ell\|_{0,\Gamma}\big). \end{aligned} \tag{4.25}$$

By substituting (4.21)-(4.25) into the error equation (4.18), using Young's inequality and choosing $\varphi^\ell=\theta_u$, $\psi^\ell=\theta_v$ we have

$$\begin{aligned} &\frac{\mathrm{d}}{\mathrm{d}t}\|\theta_u\|^2_{0,\Omega}+d_u|\theta_u|^2_{1,\Omega}+\frac{\mathrm{d}}{\mathrm{d}t}\|\theta_v\|^2_{0,\Gamma}+d_v|\theta_v|^2_{1,\Gamma} \\ &\leq C(U,u,\dot{u},v,\dot{v},d_u)\left(h^4+\|\theta_u\|^2_{0,\Omega}+\|\theta_v\|^2_{0,\Gamma}\right)+d_u|\theta_u|^2_{1,\Omega}. \end{aligned} \tag{4.26}$$

From the stability estimates (4.1)-(4.2), $\|U\|_{1,\Omega_h}$ can be bounded in terms of the norms of the initial data $\|U_0\|_{1,\Omega_h}$ and $\|V_0\|_{1,\Gamma_h}$, which in turn depend on the exact initial condition (u_0,v_0) thanks to (3.53). We can then remove the dependence of C on U in (4.26) obtaining

$$\frac{\mathrm{d}}{\mathrm{d}t}\|\theta_u\|^2_{0,\Omega}+\frac{\mathrm{d}}{\mathrm{d}t}\|\theta_v\|^2_{0,\Gamma}\leq C(u,\dot{u},v,\dot{v},d_u)\left(h^4+\|\theta_u\|^2_{0,\Omega}+\|\theta_v\|^2_{0,\Gamma}\right), \tag{4.27}$$

where $C(u,\dot{u},v,\dot{v},d_u)$ is a linear combination of the norms of the arguments between brackets. Thanks to (2.3), such a time-dependent linear combination $C(u,\dot{u},v,\dot{v},d_u)$ appearing in (4.27) fulfils

$$\int_0^T C(u,\dot{u},v,\dot{v},d_u)\mathrm{d}t<+\infty. \tag{4.28}$$

By applying Grönwall's lemma to (4.27), accounting for the h^2-accuracy of the initial conditions (3.53) and exploiting (4.28), we get the desired estimate (4.14). □

Remark 4.1 (Optimal convergence for bulk-only PDEs)**.** If the function s in (2.1) depends only on u, i.e. $s=s(u)$, then the first equation in (2.1) becomes completely decoupled from the surface PDE and takes the form

$$\begin{cases} \dot{u}-d_u\Delta u=q(u), & \boldsymbol{x}\in\Omega,\ \ t\in[0,T]; \\ \nabla u\cdot\boldsymbol{\nu}-s(u)=0, & \boldsymbol{x}\in\Gamma,\ \ t\in[0,T], \end{cases} \tag{4.29}$$

a reaction-diffusion PDE endowed with general nonlinear Robin boundary conditions. Thanks to the usage of completely distinct and decoupled Ritz projections in the bulk domain Ω and on the surface Γ, the proposed analysis applies to the bulk PDE problem

(4.29) and implies that bulk VEM in 3D retain optimal convergence in the presence of a curved boundary Γ. This result, albeit intuitive, lacked a rigorous justification in the literature. In the special case of tetrahedral meshes (FEM), the result was proven in [7]. As for VEM, previous works addressed the geometric variational crime through the usage of curved elements (see [13] for the 2D case and [28] for a mixed formulation of the Darcy problem in 3D) or through algebraic corrections in the method [16].

5 Time discretisation

In this section we will show a matrix-vector formulation of the spatially discrete formulation (3.52), and then we will show a simple and effective time discretisation scheme. By expressing the time-dependent semi-discrete solution (U,V) in the Lagrange bases

$$U(\boldsymbol{x},t)=\sum_{i=1}^{N}\lambda_i(t)\varphi_i(\boldsymbol{x}),\quad \boldsymbol{x}\in\Omega_h;\quad \text{and}\quad V(\boldsymbol{x},t)=\sum_{k=1}^{M}\mu_k(t)\psi_k(\boldsymbol{x}),\quad \boldsymbol{x}\in\Gamma_h,$$

where $\lambda_i(0)=U_0(\boldsymbol{x}_i)$ and $\mu_k(0)=V_0(\boldsymbol{x}_k)$ according to the initial condition (3.53). By using the consistency properties (3.50)-(3.51) in the approximation of the reaction kinetics, the fully discrete problem can be written as an $(M+N)\times(M+N)$ nonlinear ODE system in matrix form:

$$\begin{cases} M_\Omega\dot{\boldsymbol{\lambda}}+A_\Omega\boldsymbol{\lambda}=K_\Omega q(\boldsymbol{\lambda})+RK_\Gamma s(R^T\boldsymbol{\lambda},\boldsymbol{\mu});\\ M_\Gamma\dot{\boldsymbol{\mu}}+A_\Gamma\boldsymbol{\mu}=K_\Gamma\left(r(R^T\boldsymbol{\lambda},\boldsymbol{\mu})-s(R^T\boldsymbol{\lambda},\boldsymbol{\mu})\right). \end{cases} \tag{5.1}$$

In the above, $\boldsymbol{\lambda}(t):=(\lambda_i,\cdots,\lambda_N)^T\in\mathbb{R}^N$, $\boldsymbol{\mu}(t):=(\mu_1,\cdots,\mu_M)^T\in\mathbb{R}^M$, while M_Γ, M_Ω, A_Γ, A_Ω, K_Γ, and K_Ω are the mass, stiffness, and consistency matrices defined in (3.46)-(3.47). For the time discretisation of the spatially discrete formulation (5.1) of the BS-RDS (2.1) we use the IMEX (IMplicit-EXplicit) Euler method. The method approximates diffusion terms implicitly and reaction- and boundary-terms explicitly, see for instance [36]. The method is first-order accurate, but combines unconditional stability for the diffusion and an immediate treatment of arbitrarily nonlinear kinetics. Given the timestep $\tau>0$ we consider the equally spaced discrete times $t_n:=n\tau$, for $n=0,\cdots,N_T$, with $N_T:=\lceil\frac{T}{\tau}\rceil$. For $n=0,\cdots,N_T$ the method looks for $\boldsymbol{\lambda}^n$ and $\boldsymbol{\mu}^n$ meant to approximate the spatially discrete solution $(\boldsymbol{\lambda}(t),\boldsymbol{\mu}(t))$ at time t_n. By proceeding as in [34], the IMEX Euler time discretisation of (5.1) yields the following sequence of linear systems

$$\begin{cases} (M_\Omega+\tau K_\Omega)\boldsymbol{\lambda}^{n+1}=M_\Omega\boldsymbol{\lambda}^n+\tau K_\Omega q(\boldsymbol{\lambda}^n)+\tau RK_\Gamma s(R^T\boldsymbol{\lambda}^n,\boldsymbol{\mu}^n);\\ (M_\Gamma+\tau K_\Gamma)\boldsymbol{\mu}^{n+1}=M_\Gamma\boldsymbol{\mu}^n+\tau K_\Gamma\left(r(R^T\boldsymbol{\lambda}^n,\boldsymbol{\mu}^n)-s(R^T\boldsymbol{\lambda}^n,\boldsymbol{\mu}^n)\right), \end{cases} \tag{5.2}$$

for $n=0,\cdots,N_T-1$, where R is the reduction matrix defined in (3.1), where $\boldsymbol{\lambda}^0=\boldsymbol{\lambda}(0)$ and $\boldsymbol{\mu}^0=\boldsymbol{\mu}(0)$.

6 Numerical examples

We provide two numerical examples to illustrate our findings. In the first example, we test the convergence rate of the BS-VEM for a linear BS-PDE whose solution is known in closed form. The second example shows the application of the BS-VEM to the simulation of bulk-surface Turing patterns in a BS-RDS known in the literature. As discussed in [46], BS-RDSs in 3D constitute a useful mathematical framework for the simulation of diverse biological processes, such as cell motility, regenerative medicine, tissue engineering and more. In both experiments, the computations are carried out with our own MATLAB implementation of the BS-VEM. For illustrative purposes, each linear system is solved with MATLAB's `mldivide` solver based on LU factorisation, significantly accelerated through MATLAB's built-in function `symamd`, dedicated to the reordering of the unknowns.

6.1 A linear bulk-surface PDE: convergence

We numerically solve the following linear parabolic BS-PDE on the unit sphere Ω in 3D:

$$\begin{cases} \dot{u}-\Delta u=-u & \text{in } \Omega\times[0,T]; \\ \dot{v}-\Delta_\Gamma v+\nabla u\cdot\boldsymbol{n}=9u+8v & \text{on } \partial\Omega\times[0,T]; \\ \nabla u\cdot\boldsymbol{n}=u+v & \text{on } \partial\Omega\times[0,T], \end{cases} \tag{6.1}$$

for final time $T=0.25$, whose exact solution is given by $u(x,y,z,t)=xyze^{-t}$ for $(x,y,z,t)\in\Omega\times[0,T]$ and $v(x,y,z,t)=2xyze^{-t}$ for $(x,y,z,t)\in\partial\Omega\times[0,T]$. The initial condition of (6.1) is the exact solution (u,v) evaluated at $t=0$. We consider a sequence of four cubic meshes, $i=1,\cdots,4$, with meshsizes $h_i=\sqrt{3}\cdot 2^{-i}$. The i-th mesh is obtained by subdividing each dimension of the cube $[-1,1]^3$ into 2^{i+1} intervals, thereby producing a cubic bounding mesh. From the cubic mesh we obtain a bulk-surface mesh of the sphere, shown in Fig. 2, as described in [35]. Correspondingly, we choose timesteps $\tau_i=2^{-2-2i}$, $i=1,2,3,4$, that decrease quadratically with the meshsize. On each mesh we solve the discrete problem, we compute the error in $L^2(\Omega)\times L^2(\Gamma)$ norm at the final time $T=0.25$ and the respective convergence rate. As shown in Table 1, the convergence in $L^2(\Omega)\times L^2(\Gamma)$ norm is optimal, i.e. quadratic in space. Moreover, since the timesteps τ_i decrease quadratically with the meshsizes h_i, the experiment also implies linear convergence in time, which is also optimal for the IMEX Euler scheme. The numerical solution at the final time obtained on the finest mesh is plotted in Fig. 2. We remark that the number of spatial degrees of freedom grows cubically with i, i.e. $N=\mathcal{O}(i^3)$, while the number of timesteps grows quadratically with i, i.e. $N_T=\mathcal{O}(i^2)$. Then, on the i-th mesh we solve $\mathcal{O}(i^2)$ linear systems of dimension $\mathcal{O}(i^3)$, hence the sudden increase in computational cost (reported in seconds for the execution time) between $i=3$ and $i=4$, see Table 1. It is outside the scope of this work to consider the usage of second-order time integrators or more efficient linear solvers. This forms part of our current research program.

Table 1: Linear parabolic BS-PDE (6.1) on the unit sphere Ω in 3D. By applying the BS-VEM-IMEX Euler scheme on a sequence of four meshes with decreasing meshsize h and timestep τ, we observe optimal quadratic spatial convergence in $L^2(\Omega)\times L^2(\Gamma)$ norm. Computational times in seconds required for the time integration are shown. N_T is the number of linear systems of dimension N that are solved on each mesh i.

i	N	h	τ	$L^2(\Omega)\times L^2(\Gamma)$ error	convergence rate	Time (s)	N_T
1	53	0.8660	6.2500e-02	4.8329e-01	-	0.00884	4
2	445	0.4330	1.5625e-02	1.5106e-01	1.6778	0.01404	16
3	3089	0.2165	3.9062e-03	4.3741e-02	1.7881	0.27196	64
4	21465	0.1083	9.7656e-04	1.1473e-02	1.9308	34.65810	256

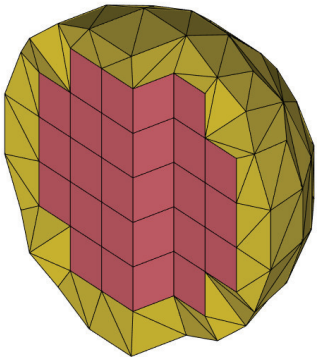

(a) Bulk-surface mesh of the sphere obtained from cubic bounding box.

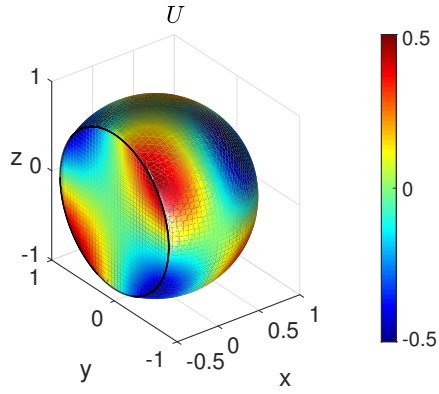

(b) U component of the numerical solution in the bulk.

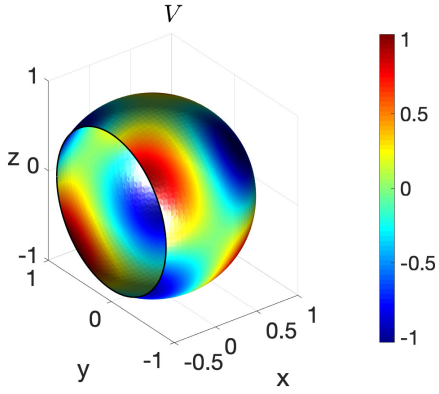

(c) V component of the numerical solution on the surface.

Figure 2: Linear parabolic BS-PDE (6.1) on the unit sphere Ω in 3D. The problem is solved on a sequence of bulk-surface meshes composed mostly of cubes like in (a) for $N=445$. The U and V components of the numerical solution obtained on the finest mesh for $i=4$ with $N=40381$ nodes and timestep $\tau=1.5625e-2$ are shown in (b) and (c).

6.2 A bulk-surface reaction-diffusion model on the sphere

We show the application of the BS-VEM to the following four-species coupled BS-RDS in 3D with *activator-depleted* kinetics considered in [46]:

$$\begin{cases} \dot{u}-\Delta u=\gamma_\Omega f(u,v) & \text{in } \Omega\times[0,T]; \\ \dot{v}-d_\Omega\Delta v=\gamma_\Omega g(u,v) & \text{in } \Omega\times[0,T]; \\ \dot{r}-\Delta_\Gamma r=\gamma_\Gamma(f(r,s)-h_1(u,v,r,s)) & \text{in } \partial\Omega\times[0,T]; \\ \dot{s}-d_\Gamma\Delta_\Gamma s=\gamma_\Gamma(g(r,s)-h_2(u,v,r,s)) & \text{in } \partial\Omega\times[0,T]; \\ \nabla u\cdot\boldsymbol{n}=\gamma_\Gamma h_1(u,v,r,s) & \text{on } \partial\Omega\times[0,T]; \\ d_\Omega\nabla v\cdot\boldsymbol{n}=\gamma_\Gamma h_2(u,v,r,s) & \text{on } \partial\Omega\times[0,T], \end{cases} \tag{6.2}$$

where $f(u,v):=a-u+u^2v$, $g(u,v):=b-u^2v$, $h_1(u,v,r,s):=\alpha_1 r-\beta_1 u-\kappa_1 v$, and $h_2(u,v,r,s):=\alpha_2 s-\beta_2 u-\kappa_2 v$. As shown in [47], the following is a spatially homogeneous steady state for system (6.2):

$$(u^*,v^*,r^*,s^*):=\Big(a+b,\frac{b}{(a+b)^2},a+b,\frac{b}{(a+b)^2}\Big). \tag{6.3}$$

The steady state (6.3) is Turing unstable under specific conditions on the parameters, which are met by the following parameter choice:

$$\begin{aligned} &a=0.1;\quad b=0.9;\quad \alpha_1=\frac{5}{12};\quad \alpha_2=5;\quad \beta_1=\frac{5}{12};\quad \beta_2=0;\quad \kappa_1=0;\quad \kappa_2=5; \\ &d_\Omega=10;\quad d_\Gamma=10;\quad \gamma_\Omega=55;\quad \gamma_\Gamma=55. \end{aligned} \tag{6.4}$$

Correspondingly, the steady state (6.3) becomes $(1,0.9,1,0.9)$. We solve the problem on the unit sphere, approximated with a polyhedral mesh with $N=5749$ nodes, with final time $T=20$, timestep $\tau=2e-4$, and initial data given as small spatially random perturbations of amplitude 1*e*-3 around the equilibrium (6.3). As we can see in Fig. 3, the solution at the time $T=20$ is a pattern with multiple symmetries. Specifically, the surface components (r,s) possess six spot patterns located at the vertexes of a cube. The bulk components (u,v), instead, show four "tunnels" connecting the top spot of (r,s) to the four equatorial spots of (r,s) and an internal spot that matches the bottom spot of (r,s).

7 Conclusions and future challenges

In this study, we have considered a bulk-surface virtual element method (BS-VEM) for the numerical approximation of coupled bulk-surface reaction-diffusion systems (BS-RDSs). The proposed method combines a 3D virtual element method (VEM) for the bulk equations [1, 10] with a surface virtual element method (SVEM) for the surface equations [38]. The special case of simplicial bulk-surface meshes encompasses the BS-FEM for BS-RDSs [46]. This work extends the work in [34], devoted to the 2D case.

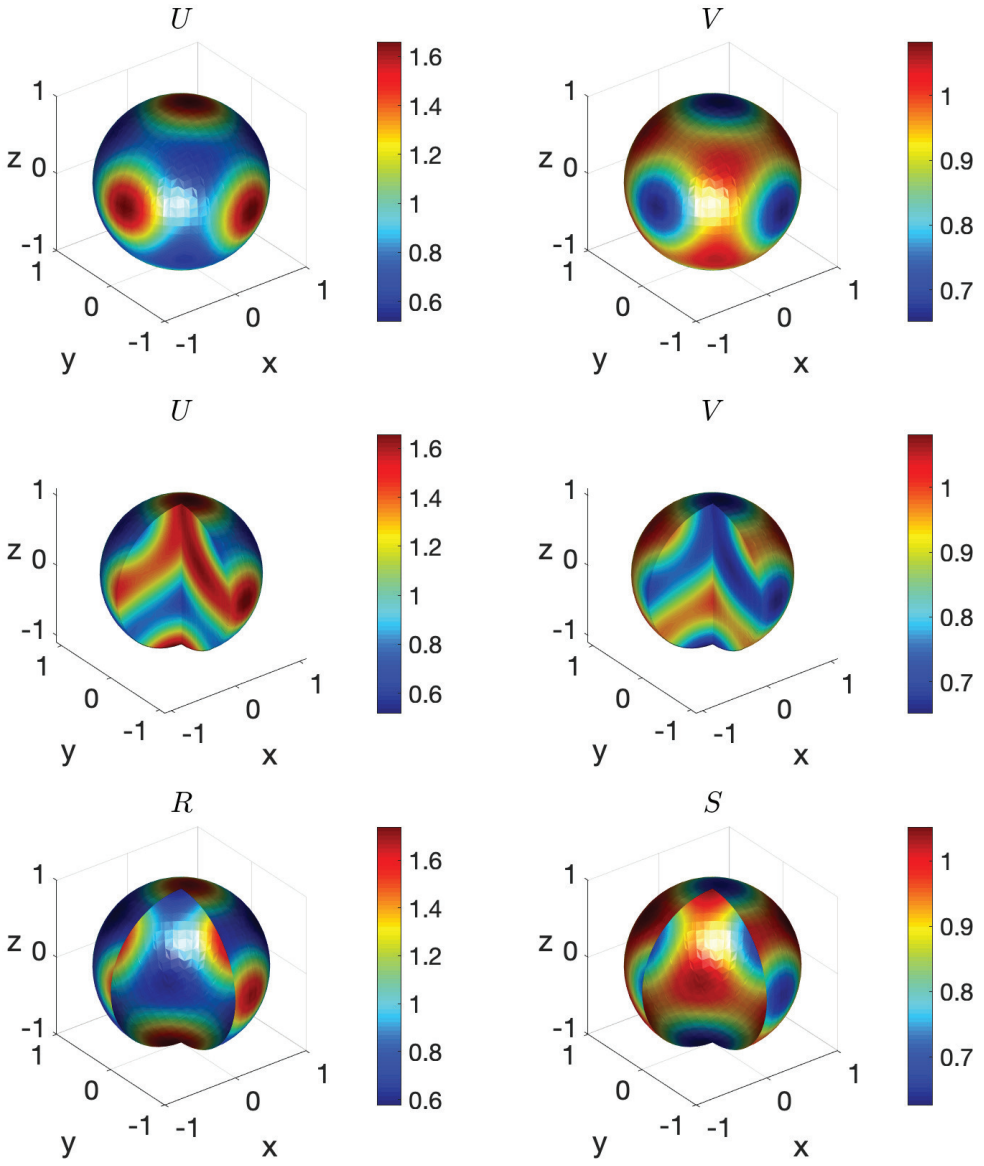

Figure 3: Numerical solution of the BS-RDS (6.2) on the unit sphere, approximated with a polyhedral mesh with $N=5749$ nodes, at the final time $T=20$, with timestep $\tau=2e$-4. Top row: bulk components (U,V). Middle row: a cross-sectional view of the bulk components (U,V). Bottom row: surface components (R,S).

We have adopted the polyhedral bulk-surface meshes considered in [35] and we have used the corresponding geometric error estimates. Exactly as in the special case of the tetrahedral meshes used in the BSFEM, the geometric error is $\mathcal{O}(h)$ in the bulk (although confined to a h-narrow band) and $\mathcal{O}(h^2)$ on the surface, where h is the meshsize.

We have carried out a full error analysis. Specifically, if the exact solution is $H^{2+\frac{3}{4}}(\Omega)$ in the bulk and $H^2(\Gamma)$ on the surface, the BS-VEM possesses optimal second-order convergence in space in L^2 norm. The present analysis combines the techniques used in [34] and [35] and contains suitable adaptations due to the simultaneous presence of nonlinearities, time dependence, and 3D.

From the properties of our bulk-Ritz projection we have drawn an additional consequence: the lowest order bulk-VEM in 3D [8] retains optimal convergence even in the simultaneous presence of curved boundaries and non-zero boundary conditions, a result that was not fully addressed in the literature, to the best of our knowledge.

We have provided two numerical examples to demonstrate (i) the optimal convergence in space and time and (ii) the simulation of Turing patterns in a known bulk-surface activator-inhibitor model system of four species.

The present work paves the way for future research directions. For instance, higher order convergence in space is an open problem. The analysis in this work indicates that the main challenge to this end is the geometric error, which could be addressed with curved 3D elements, following the seminal work in [28]. Another future direction is the extension to evolving domains. Both of these challenges form part of our current studies.

Acknowledgments

The work of MF was funded by Regione Puglia (Italy) through the research programme REFIN-Research for Innovation (protocol code 901D2CAA, project No. UNISAL026). MF acknowledges support from the Italian National Institute of High Mathematics (INdAM) through the INdAM-GNCS Project no. CUP E55F22000270001. This work (AM) was partly supported by the Global Challenges Research Fund through the Engineering and Physical Sciences Research Council grant number EP/T00410X/1: UK-Africa Postgraduate Advanced Study Institute in Mathematical Sciences, the Health Foundation (1902431), the NIHR (NIHR133761) and by the Discovery Grant awarded by Canadian Natural Sciences and Engineering Research Council (2023–2028). AM acknowledges support from the Royal Society Wolfson Research Merit Award funded generously by the Wolfson Foundation (2016-2021). AM is a Distinguished Visiting Scholar to the Department of Mathematics, University of Johannesburg, South Africa, and the University of Pretoria in South Africa. IS and MF are members of the INdAM-GNCS activity group. The work of IS is supported by the PRIN 2020 research project (no. 2020F3NCPX) "Mathematics for Industry 4.0", and from the "National Centre for High Performance Computing, Big Data and Quantum Computing" funded by European Union – NextGenerationEU, PNRR project code CN00000013, CUP F83C22000740001.

Appendix: Definitions and basic results

In this Appendix we provide preliminary definitions, results and notations adopted throughout the article. We start by introducing some notation on Lebesgue and Sobolev

spaces. If $p\in[1,+\infty]$, we denote by $L^p(\Omega)$ and $L^p(\Gamma)$ the usual Lebesgue spaces on Ω and Γ, with $\|\cdot\|_{0,p,\Omega}$ and $\|\cdot\|_{0,p,\Gamma}$ being the respective norms. If $m\in\mathbb{N}$ and $p\in[1,+\infty]$, we denote by $W^{m,p}(\Omega)$ and $W^{m,p}(\Gamma)$ the usual Sobolev spaces of integer order m on Ω and Γ, with $\|\cdot\|_{m,p,\Omega}$ and $\|\cdot\|_{m,p,\Gamma}$ being the respective norms. Finally, for $s\in[0,+\infty)$ and $p\in[1,+\infty)$, we denote by $W^{s,p}(\Omega)$ and $W^{s,p}(\Gamma)$ the Sobolev Spaces of fractional order s on Ω and Γ, with $\|\cdot\|_{s,p,\Omega}$ and $\|\cdot\|_{s,p,\Gamma}$ being the respective norms, see [35] for full definitions. In the notable case $p=2$, we adopt the usual notation $H^s:=W^{s,2}$ and $\|\cdot\|_{s,\Omega}$ or $\|\cdot\|_{s,\Gamma}$ for the respective norms. The following results are used throughout the analysis.

Lemma A.1 (Inclusion between fractional Sobolev spaces, [29]). *Let $\Omega\subset\mathbb{R}^3$ be a bounded domain with a $\mathcal{C}^1$ boundary[§] Γ, let $p\in[1,+\infty)$ and $s,s'\in[0,+\infty)$ such that $s<s'$. Then there exists $C>0$ depending on Ω and s such that*

$$\|u\|_{s,p,\Omega}\leq C\|u\|_{s',p,\Omega}, \tag{A.1}$$

for all $u\in W^{s',p}(\Omega)$. Hence, $W^{s,p}(\Omega)\subset W^{s',p}(\Omega)$.

Theorem A.1 (Narrow band trace inequality, [31]). *For $\delta>0$ let U_δ be the* narrow band of Γ of width δ *(see [35] for a full definition and Fig. 1(a) for an illustration). There exists $C>0$ (depending on Ω) such that if δ is sufficiently small (depending on Ω), then any $u\in H^1(\Omega)$ fulfils*

$$\|u\|_{0,U_\delta}\leq C\delta^{\frac{1}{2}}\|u\|_{1,\Omega}. \tag{A.2}$$

Theorem A.2 (Trace theorem, [53, 54]). *Let $k\in\mathbb{N}$, $1/2<s\leq k$ and assume that the boundary Γ is a $\mathcal{C}^k$ surface.[¶] Then there exists a bounded operator* $\mathrm{Tr}:H^s(\Omega)\to H^{s-1/2}(\Gamma)$, *called the* trace operator, *such that $\mathrm{Tr}(u)=u_{|\Gamma}$. The trace operator fulfils*

$$\|\mathrm{Tr}(u)\|_{s-\frac{1}{2},\Gamma}\leq C\|u\|_{s,\Omega},\quad\forall\, u\in H^s(\Omega). \tag{A.3}$$

Theorem A.3 (Stein extension theorem, [54, Chap. 6, Theorem 5]). *Let $\Omega\subset\mathbb{R}^3$ have a Lipschitz boundary Γ, let $r\in\mathbb{N}$ and $p\in[1,+\infty]$. Then, there exists $C>0$, depending on Ω and r but not on p, such that, for any $u\in W^{r,p}(\Omega)$, there exists $\tilde{u}\in W^{r,p}(\mathbb{R}^3)$ fulfilling $\tilde{u}_{|\Omega}=u$ and*

$$\|\tilde{u}\|_{r,p,\mathbb{R}^3}\leq C\|u\|_{r,p,\Omega}. \tag{A.4}$$

References

[1] D Adak, E Natarajan, and S Kumar. Convergence analysis of virtual element methods for semilinear parabolic problems on polygonal meshes. *Numer. Methods Partial Differ. Equ.*, 35(1):222–245, 2019. doi:10.1002/num.22298.

[§]See [35] for a full definition of $\mathcal{C}^k$ surfaces.

[¶]It suffices that Γ is a $\mathcal{C}^{k-1,1}$ surface meaning that the derivatives of its local charts up to order $k-1$ are Lipschitz continuous. For simplicity, we make the stronger assumption that $\Gamma\in\mathcal{C}^k$.

[2] B Ahmad, A Alsaedi, F Brezzi, L D Marini, and A Russo. Equivalent projectors for virtual element methods. *Comput. Math. with Appl.*, 66(3):376–391, 2013. doi:10.1016/j.camwa.2013.05.015.

[3] H Amann. Existence and regularity for semilinear parabolic evolution equations. *Ann. Sc. Norm. Super. Pisa Cl. Sci.*, 11(4):593–676, 1984. url:http://www.numdam.org/item/ASNSP_1984_4_11_4_593_0/.

[4] P F Antonietti, L Beirão Da Veiga, S Scacchi, and M Verani. A C^1 virtual element method for the Cahn-Hilliard equation with polygonal meshes. *SIAM J. Numer. Anal.*, 54(1):34–56, 2016. doi:10.1137/15m1008117.

[5] D Autovino, M Minacapilli, and G Provenzano. Modelling bulk surface resistance by modis data and assessment of MOD16A2 evapotranspiration product in an irrigation district of southern Italy. *Agric. Water Manag.*, 167:86–94, 2016. doi:10.1016/j.agwat.2016.01.006.

[6] E Bachini, G Manzini, and M Putti. Arbitrary-order intrinsic virtual element method for elliptic equations on surfaces. *Calcolo*, 58(3):1–28 2011. doi:10.1007/s10092-021-00418-5.

[7] S. Bartels, C. Carstensen, and G. Dolzmann. Inhomogeneous Dirichlet conditions in a priori and a posteriori finite element error analysis. *Numer. Math.*, 99(1):1–24, 2004. doi:10.1007/s00211-004-0548-3.

[8] L Beirão Da Veiga, F Brezzi, A Cangiani, G Manzini, L D Marini, and A Russo. Basic principles of virtual element methods. *Math. Models Methods Appl. Sci.*, 23(01):199–214, 2013. doi:10.1142/S0218202512500492.

[9] L Beirão Da Veiga, F Brezzi, and L D Marini. Virtual elements for linear elasticity problems. *SIAM J. Numer. Anal.*, 51(2):794–812, 2013. doi:10.1137/120874746.

[10] L Beirão Da Veiga, F Dassi, and A Russo. High-order virtual element method on polyhedral meshes. *Comput. Math. with Appl.*, 74(5):1110–1122, 2017. doi:10.1016/j.camwa.2017.03.021.

[11] L Beirão Da Veiga, C Lovadina, and G Vacca. Divergence free virtual elements for the Stokes problem on polygonal meshes. *ESAIM: Math. Model. Numer. Anal.*, 51(2):509–535, 2017. doi:10.1051/m2an/2016032.

[12] L Beirão Da Veiga and G Manzini. A virtual element method with arbitrary regularity. *IMA J. Numer. Anal.*, 2013. doi:10.1093/imanum/drt018.

[13] L Beirão Da Veiga, A Russo, and G Vacca. The virtual element method with curved edges. *ESAIM: Math. Model. Numer. Anal.*, 53(2):375–404, 2019. doi:10.1051/m2an/2018052.

[14] M F Benedetto, S Berrone, and S Scialò. A globally conforming method for solving flow in discrete fracture networks using the virtual element method. *Finite Elem. Anal. Des.*, 109:23–36, 2016. doi:10.1016/j.finel.2015.10.003.

[15] N Benkemoun, A Ibrahimbegovic, and J-B Colliat. Anisotropic constitutive model of plasticity capable of accounting for details of meso-structure of two-phase composite material. *Comput. Struct.*, 90:153–162, 2012. doi:10.1016/j.compstruc.2011.09.003.

[16] S Bertoluzza, M Pennacchio, and D Prada. High order VEM on curved domains. *Rendiconti Lincei - Matematica e Applicazioni*, 30:391–412, 2019. doi:10.4171/RLM/853.

[17] S Bianco, F Tewes, L Tajber, V Caron, O I Corrigan, and A M Healy. Bulk, surface properties and water uptake mechanisms of salt/acid amorphous composite systems. *Int. J Pharm.*, 456(1):143–152, 2013. doi:10.1016/j.ijpharm.2013.07.076.

[18] J Borgqvist, A Malik, C Lundholm, A Logg, P Gerlee, and M Cvijovic. Cell polarisation in a bulk-surface model can be driven by both classic and non-classic turing instability. *NPJ Syst. Biol. Appl.*, 7(1):1–10, 2021. doi:10.1038/s41540-021-00173-x.

[19] F Brezzi and L D Marini. Virtual element methods for plate bending problems. *Comput.*

Methods Appl. Mech. Eng., 253:455–462, 2013. doi:10.1016/j.cma.2012.09.012.

[20] E Burman, P Hansbo, M Larson, and S Zahedi. Cut finite element methods for coupled bulk–surface problems. *Numer. Math.*, 133(2):203–231, 2016. doi:10.1007/s00211-015-0744-3.

[21] A Cangiani, E H Georgoulis, and S Metcalfe. Adaptive discontinuous Galerkin methods for nonstationary convection–diffusion problems. *IMA J. Numer. Anal.*, 34(4):1578–1597, 2014. doi:10.1093/imanum/drt052.

[22] J Chen. A memory efficient discontinuous Galerkin finite-element time-domain scheme for simulations of finite periodic structures. *Microw. Opt. Technol. Lett.*, 56(8):1929–1933, 2014. doi:10.1002/mop.28483.

[23] M Chen and L Ling. Kernel-based meshless collocation methods for solving coupled bulk–surface partial differential equations. *J. Sci. Comput.*, 81(1):375–391, 2019. doi:10.1007/s10915-019-01020-2.

[24] A Y Chernyshenko, M A Olshanskii, and Y V Vassilevski. A hybrid finite volume–finite element method for bulk–surface coupled problems. *J. Comput. Phys.*, 352:516–533, 2018. doi:10.1016/j.jcp.2017.09.064.

[25] J A Cottrell and T J R Hughes and Y Bazilevs *Isogeometric Analysis: Toward Integration of CAD and FEA*. John Wiley & Sons, 2009. doi:10.1002/9780470749081.

[26] D Cusseddu, L Edelstein-Keshet, J A Mackenzie, S Portet, and A Madzvamuse. A coupled bulk-surface model for cell polarisation. *J. Theor. Biol.*, 481:119–135, 2019. doi:10.1016/j.jtbi.2018.09.008.

[27] KY Dai, GR Liu, and TT Nguyen. An n-sided polygonal smoothed finite element method (nSFEM) for solid mechanics. *Fin Elem. Anal. Des.*, 43(11):847–860, 2007. doi:10.1016/j.finel.2007.05.009.

[28] F Dassi, A Fumagalli, A Scotti, and G Vacca. Bend 3D mixed virtual element method for Darcy problems. *Comput. Math. with Appl.*, 119:1–12, 2022. doi:10.1016/j.camwa.2022.05.023.

[29] E Di Nezza, G Palatucci, and E Valdinoci. Hitchhiker's guide to the fractional Sobolev spaces. *Bull. des Sci. Math.*, 136(5):521–573, 2012. doi:10.1016/j.bulsci.2011.12.004.

[30] G Dziuk and C M Elliott. Finite element methods for surface PDEs. *Acta Numerica*, 22:289–396, 2013. doi:10.1017/s0962492913000056.

[31] C M Elliott and T Ranner. Finite element analysis for a coupled bulk–surface partial differential equation. *IMA J. Numer. Anal.*, 33(2):377–402, 2013. doi:10.1093/imanum/drs022.

[32] C M Elliott and T Ranner. Evolving surface finite element method for the Cahn–Hilliard equation. *Numer. Math.*, 129(3):483–534, 2014. doi:10.1007/s00211-014-0644-y.

[33] C M Elliott, T Ranner, and C Venkataraman. Coupled bulk-surface free boundary problems arising from a mathematical model of receptor-ligand dynamics. *SIAM J. Math. Anal.*, 49(1):360–397, Jan 2017. doi:10.1137/15m1050811.

[34] M Frittelli, A Madzvamuse, and I Sgura. Bulk-surface virtual element method for systems of PDEs in two-space dimensions. *Numer. Math.*, 147(2):305–348, 2021. doi:10.1007/s00211-020-01167-3.

[35] M Frittelli, A Madzvamuse, and I Sgura. Virtual element method for elliptic bulk-surface PDEs in three space dimensions. *Numer. Methods Partial Differ. Equ.*, Accepted for publication.

[36] M Frittelli, A Madzvamuse, I Sgura, and C Venkataraman. Preserving invariance properties of reaction–diffusion systems on stationary surfaces. *IMA J. Numer. Anal.*, 39(1):235–270, 2017. doi:10.1093/imanum/drx058.

[37] M Frittelli, A Madzvamuse, I Sgura, and C Venkataraman. Numerical preservation of ve-

locity induced invariant regions for reaction–diffusion systems on evolving surfaces. *J. Sci. Comput.*, 77(2):971–1000, 2018. doi:10.1007/s10915-018-0741-7.

[38] M Frittelli and I Sgura. Virtual element method for the Laplace-Beltrami equation on surfaces. *ESAIM: Math. Model. Numer. Anal.*, 52(3):965–993, 2018. doi:10.1051/m2an/2017040.

[39] A Fumagalli, A Scotti, and L Formaggia. Performances of the mixed virtual element method on complex grids for underground flow. In *Polyhedral Methods in Geosciences*, pages 299–329. Springer, Cham, 2021. doi:10.1007/978-3-030-69363-3_8.

[40] S Gómez. High-order interpolatory Serendipity Virtual Element Method for semilinear parabolic problems. *Calcolo*, 59(3):1–27, 2022. doi:10.1007/s10092-022-00468-3.

[41] S Gross, M A Olshanskii, and A Reusken. A trace finite element method for a class of coupled bulk-interface transport problems. *ESAIM: Math. Model. Numer. Anal.*, 49(5):1303–1330, 2015. doi:10.1051/m2an/2015013.

[42] B Kovács and C Lubich. Numerical analysis of parabolic problems with dynamic boundary conditions. *IMA J. Numer. Anal.*, 37(1):1–39, May 2017. doi:10.1093/imanum/drw015.

[43] D Lacitignola, M Frittelli, V Cusimano, and A De Gaetano. Pattern formation on a growing oblate spheroid. An application to adult sea urchin development. *J. Comput. Dyn.*, 9(2):185, 2022. doi:10.3934/jcd.2021027.

[44] A A Lee, A Münch, and E Süli. Degenerate mobilities in phase field models are insufficient to capture surface diffusion. *Appl. Phys. Lett.*, 107(8):081603, Aug 2015. doi:10.1063/1.4929696.

[45] J A Mackenzie, M Nolan, and R H Insall. Local modulation of chemoattractant concentrations by single cells: Dissection using a bulk-surface computational model. *Interface Focus*, 6(5):20160036, 2016. doi:10.1098/rsfs.2016.0036.

[46] A Madzvamuse and A H W Chung. The bulk-surface finite element method for reaction–diffusion systems on stationary volumes. *Finite Elem. Anal. Des.*, 108:9–21, Jan 2016. doi:10.1016/j.finel.2015.09.002.

[47] A Madzvamuse, A H W Chung, and C Venkataraman. Stability analysis and simulations of coupled bulk-surface reaction-diffusion systems. *Proc. R. Soc. A: Math. Phys. Eng. Sci.*, 471(2175):20140546–20140546, Feb 2015. doi:10.1098/rspa.2014.0546.

[48] D Mora, G Rivera, and R Rodríguez. A virtual element method for the Steklov eigenvalue problem. *Math. Models Methods Appl. Sci.*, 25(08):1421–1445, 2015. doi:10.1142/s0218202515500372.

[49] L Murphy and A Madzvamuse. A moving grid finite element method applied to a mechanobiochemical model for 3d cell migration. *Appl. Numer. Math.*, 158:336–359, 2020. doi:10.1016/j.apnum.2020.08.004.

[50] F Paquin-Lefebvre, W Nagata, and M J Ward. Pattern formation and oscillatory dynamics in a two-dimensional coupled bulk-surface reaction-diffusion system. *SIAM J. Appl. Dyn. Syst.*, 18(3):1334–1390, 2019. doi:10.1137/18m1213737.

[51] A Rätz and M Röger. Symmetry breaking in a bulk–surface reaction–diffusion model for signalling networks. *Nonlinearity*, 27(8):1805–1827, Jul 2014. doi:10.1088/0951-7715/27/8/1805.

[52] L S Ryder, Y F Dagdas, M J Kershaw, C Venkataraman, A Madzvamuse, et al. A sensor kinase controls turgor-driven plant infection by the rice blast fungus. *Nature*, 574(7778):423–427, 2019. doi:10.1038/s41586-019-1637-x.

[53] S.L. Sobolev. *Partial Differential Equations of Mathematical Physics*. Pergamon Press, London, 1964. doi:10.1016/c2013-0-01785-9.

[54] E M Stein. *Singular Integrals and Differentiability Properties of Functions (PMS-30)*. Princeton

University Press, Princeton, 1971. doi:10.1515/9781400883882.

[55] G Vacca. Virtual element methods for hyperbolic problems on polygonal meshes. *Comput. Math. with Appl.*, 2016. doi:10.1016/j.camwa.2016.04.029.

[56] G Vacca and L Beirão Da Veiga. Virtual element methods for parabolic problems on polygonal meshes. *Numer. Methods Partial Differ. Equ.*, 31(6):2110–2134, 2015. doi:10.1002/num.21982.